European volcanological supersite in Iceland: a monitoring system and network for the future

Report

D7.2 – Field laboratory, aircraft observations and radars

Work Package:	*Determination and evolution of eruption source parameters*
Work Package number:	*7*
Deliverable:	*Field laboratory, aircraft observations and radars*
Deliverable number:	*7.2*
Type of Activity:	*RTD*
Responsible activity leader:	*Magnús T. Gudmundsson*
Responsible participant:	*UI*
Authors:	*Magnús T. Gudmundsson (UI),Thórdís Högnadóttir (UI), Tobias Dürig (UI),Ármann Höskuldsson (UI), Halldór Björnsson (IMO), Björn Oddsson (NCIP-DCPEM), Thorbjörg Ágústsdóttir (formerly at UI)*

Type of Deliverable:	*Report*	*[x]*	*Demonstrator*	*[ ]*
	Prototype	*[ ]*	*Other*	*[ ]*
Dissemination level:	*Public*	*[x]*	*Restricted Designated Group*	*[ ]*
	Prog. Participants (FP7)	*[ ]*	*Confidential (consortium)*	*[ ]*

Seventh Framework Programme
EC project number: 308377

Abstract

This report deals with three issues of effective monitoring of eruptions and interpretation of eruption plume data to obtain mass eruption rates (MER). Part I is on the Mobile Field Laboratory, Part II on best practices in eruption monitoring from aircraft, and Part III is on comparison of plume model predictions with observed fallout in the explosive eruption of Eyjafjallajökull 2010. The first two parts belong to Task 7.2 and the final part to Task 7.3 in WP7 in FUTUREVOLC.

Part I: The Mobile Field Lab is a set of instruments and tools that has been partly obtained within the FUTUREVOLC project, and partly existed at the Institute of Earth Sciences. These tools and instruments are assembled in such a way that they can be quickly taken from their usual locations in the laboratories and transported to a temporary laboratory or facility set up where samples can be taken and eruption monitoring carried out. This will speed up the delivery of important information, e.g. in an explosive eruption on magma composition, tephra grain sizes and shape characteristics. The mobile lab include a particle analyser, sieves for grain size analyses, a mobile X-ray chemical analyser, Scanning electron microscope (SEM), and digital video and still cameras.

Part II: Eruptions in Iceland often take place in very inaccessible areas, including within glaciers. A crucial part of monitoring has been aircraft observations. Over the years methods specific for e.g. subglacial eruptions have been developed and these methods were applied in all recent eruptions, including the Eyjafjallajökull eruption in 2010, the Grímsvötn eruption in 2011 and the recent Bárðarbunga eruption of 2014-15. The best practices manual presented here, is an updated version of prototype version 1, presented as Milestone 62 in FUTUREVOLC. Methods and checklists for both volcanological and meteorological observations in eruptions in different settings are presented. These settings are: Explosive eruptions, terrestrial effusive eruptions, subglacial/englacial eruptions, submarine to emergent eruptions and jökulhlaups. It also contains information on aircraft used, the mounting of videos and cameras, and reporting to civil authorities.

Part III: This section presents analysis of empirical data on mass erupted and plume height in the eruption of Eyjafjallajökull in 2010. This was initially planned as part of Deliverable 7.1 but was moved to D7.2 while reporting of radar for plume monitoring was moved from D7.2 to D7.1. The near-continuous record of plume height from the C-band radar in Keflavík airport, 155 km away from Eyjafjallajökull is calibrated using 77 pairs of photo-derived plume heights and radar retrievals. The result is that a best fit is obtained with a 0.5 km increase in radar-derived heights. This corrected record is used to calculate the MER and predicted mass erupted for five different phases of the eruption. The predicted mass is then compared with fallout as measured on the ground and estimated fallout out to sea. It is found that the simple empirical models of "Sparks" and "Mastin" together with a theoretical simple buoyancy model ("Wilson") give results similar to the measured fallout, while plume models incorporating wind effect predict up to an order of magnitude higher mass than observed. The effect of wind on plume height is nevertheless seen in the data, suggesting that proper calibration of wind-effect in models should occur before their effective incorporation into operational MER systems.

I. Mobile field laboratory

Ármann Höskuldsson
Nordvulk, Institute of Earth Sciences, University of Iceland

Introduction – overview

The mobile laboratory of Futurevolc is thought as a rapid response unit in case of a volcanic eruption. In most cases the instruments needed for analysis are located in laboratories at Universities or institutions that are called up on in case of volcanic unrest. Thus analytical instruments are usually located at hundreds of kilometres distance from the actual crisis area. This means that considerable time has to be used for transport of samples, causing delay between observations and analysis. By equipping the onsite observation team with mobile instruments capable to do first analysis and interpretations on deposits and course of events on site, crucial time between observation and response is shortened. The instruments of the mobile lab are located at the Institute of Earth Sciences in Reykjavik between eruptions where they are used for various research, not least on aspects of previous eruptions.

Futurevolc and the mobile laboratory are thus thought to answer the need of shortening observation and interpretation time. Although at the time of proposal writing the mobile lab was first and foremost planned for explosive eruptions, the equipment was shown to be useful in the last eruption in Iceland (2014-2015) that was of the effusive type.

The mobile lab consists of many different instruments, part of which the Futurevolc program supports and other that were already in the possession of the Institute of Earth Science. This includes tools, simple as hammers, shovels, meters, computers and GPS instruments. However, in this report we shall not go through the total arsenal of the mobile lab, but focus on the instruments obtained by the support of the Futurevolc program and the ones considered critical for mobile lab quick response, namely (1) particle analyser, (2) Scanning Electron Microscope, (3) mobile X-ray chemical analyser, (4) GoPro video cameras, (5) digital cameras, (6) sieves, for grain size analysis. The Futurvolc program supported also design and making of an Automated tephra sampler to be deployed in the field in areas of active thephra fall. That instrument is described in detail in Deliverable Report 7.3.

1. Scanning electron microscope (SEM)

The scanning electron microscope (SEM) that was chosen for the mobile lab is of the Hitachi TM3000 table top type. It was carefully selected after going through tests of the available table top SEM microscopes on the marked. The microscope is extremely easy to handle, small and can be set up in any place, as long as there is electricity available (mobile generator or national network). Samples need minimal handling prior to analysis. The analytical work that can be done is both visual and chemical, thus enabling the onsite team to determine grain shapes, magma and or crystal chemistry.

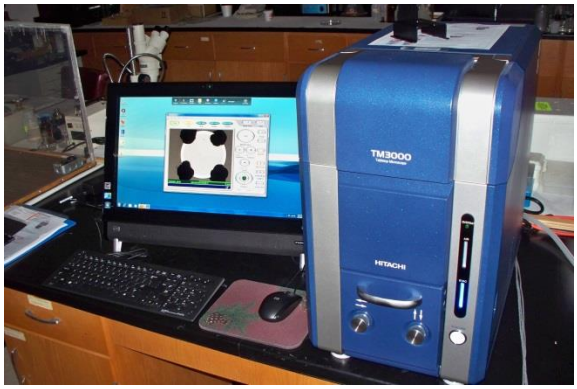

Figure 1a The Hitachi TM3000 table top scanning electron microscope. The instrument can be packed for transport in a short time. Due to its compact size it can also be easily transported between the institute and crisis site.

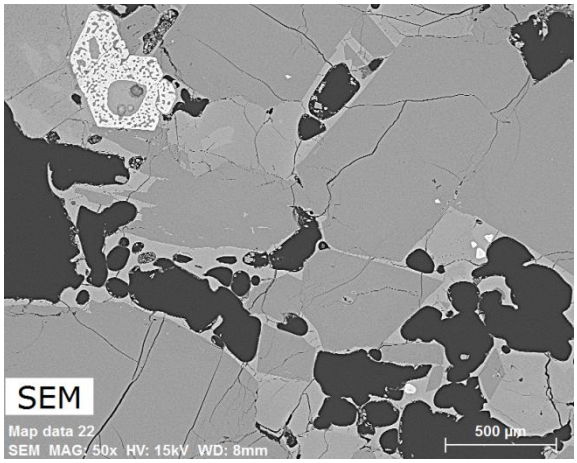

Figure 1b An example of an immage obtained by the TM3000. The image shows a tephra grain. The grain is composed of crystals, magmatic glass and voids representing the gas-blisters in the magma.

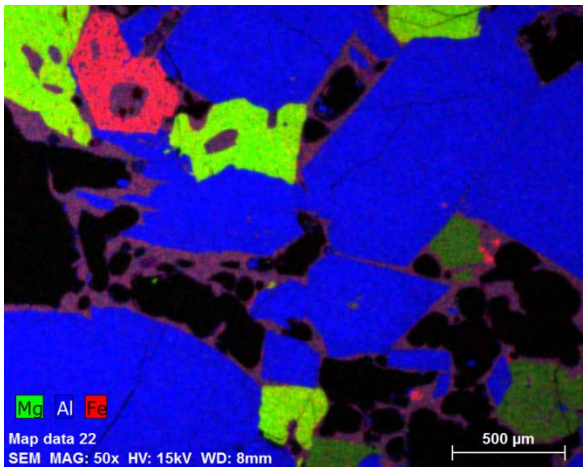

Figure 1c Chemical map of the same tephra grain as in Figure 1b Elements illustrated are Magnesium, Aluminium and Iron. Aluminium (in blue) shows the presence of plagioclase crystals, Magnesium (in green) shows the presence of olivine crystals and Iron (in red) shows the presence of iron minerals, in this case magnetite.

The SEM proofed to be crucial during the 2014-2015 eruption, since no other rapid analytical equipment was working in the country at the time.

2. Mobile handheld XRF spectrometer

The handheld XRF solution selected for the mobile lab was the S1 TITAN from Bruker. It is among the lightest (1.5 kg, including battery) tube-based handheld XRF analysers on the market today. Fast analysis speed and exceptional accuracy are two key reasons the instrument was chosen. Other innovative features include an integrated touch-screen colour display, 50 kV X-ray tube, SMART Grade™ timing, SharpBeam™ optimized X-ray geometry, Silicon Drift Detector (SDD), and an extremely tough housing that is sealed against humid and dusty environments. It is also calibrated for silica rocks that make it extremely useful for the onsite team.

The XRF gun is mainly to be used in explosive eruptions, where rapid changes in chemistry of the tephra can be expected and rapid communication on such changes need to happen between field teams and the crisis management centre. The instrument was not needed in last eruption crisis in Iceland.

Figure 2a Handheld XRF for rapid chemical analysis in the field. Instrument is small an easily transportable.

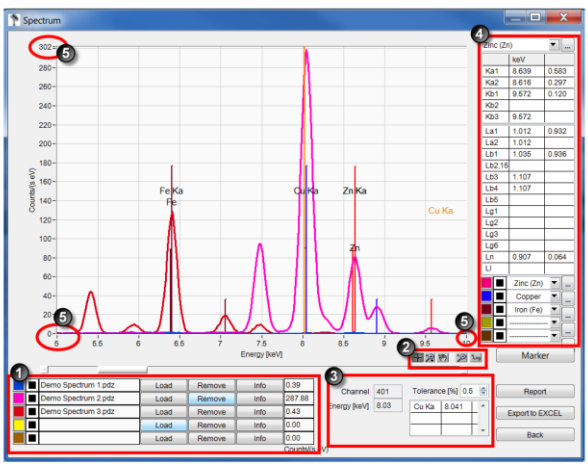

Figure 2b View from the analytical software of Titan S1 XRF. It shows the quantitated element abundance in the sample being analyzed. The XRF offers unique opportunity to make quick first chemical analysis in the field during crisis.

3. Particle analyser

The Particle Insight is a state-of-the art dynamic image analyser which is ideal for applications where the shape of raw materials, not just the diameter, is critical. The Particle Insight offers up to 28 different shape parameters analysed and reported real-time for samples in either aqueous or organic solvent suspensions. The system operates in a range suitable for geological specimens from 3 µm up to 300 µm in its standard configuration. Its unique recirculating sample module and precision optics are designed to acquire and report statistically valid measurements quickly.

In case of explosive eruptions the shape of grains produced is critical. Among other the grain shape will affect the floating ability of the grains and therefore the possibility of grains to reach far from the eruption site. In many cases tephra grains can be transported over several thousand kilometers, thus remote volcanoes can have an effect in distant populated areas.

The particle and shape analyser has the capacity to analyse more than 16000 grains in just 5 min. This makes the statistical correctness of measurement sound and avoids human skewness in the measurement.

Figure 3a The particle shape analyzer is small and compact and can be easily dismounted and deployed out in the field.

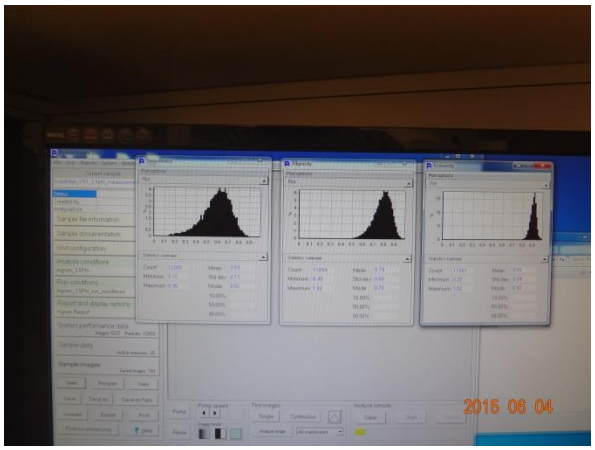

Figure 3b Example, of results obtained by the shape analyzer. The analyzer can do more than 16 thousand grains in just 5 min. Thus the statistical correctness of shape analyzing reliable.

4. Sieves for grain size analysis

Sets of sieves suitable for tephra grain size analysis is exist at the Institute of Earth Sciences, covering grain sizes from 64 mm down to 63 µm. These sieves are always ready for transport as a part of the mobile lab, when the need arises.

Figure 4a Complete set of sieves from 64 mm to 0.063 mm is at hand for the mobile lab in case of crisis. The aim is to do first assessment of grain size distribution in the eruption cloud as quickly as possible.

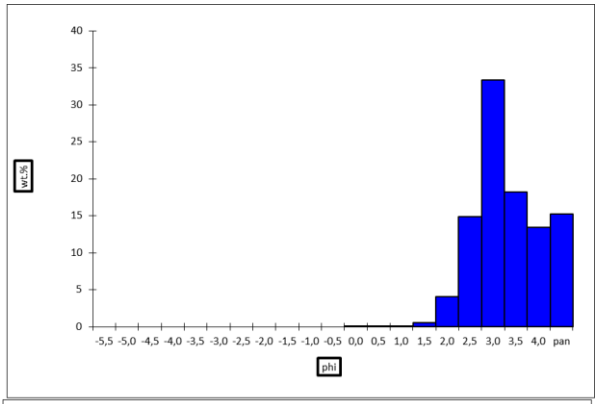

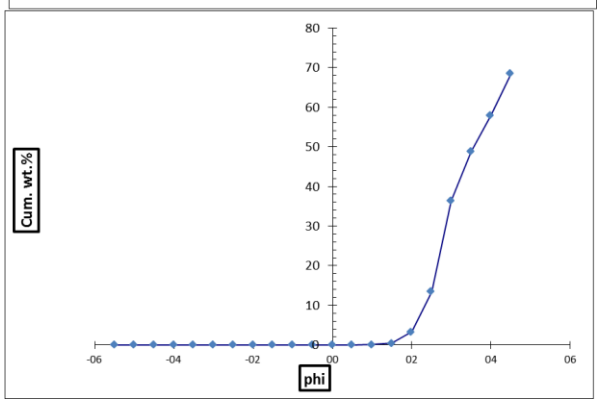

Figure 4b Example of sample sieved during the eruption crisis of Grimsvötn Iceland in 2011. The sample is taken from about 65 km distance to vent. Very high quantites of fines characterizes distal deposits in explosive eruptions.

5. Automated tephra sampler

This instrument has been explained in Deliverable report 7.3. The mobile lab has had one out of five instruments since September 2014. However, the eruption in Bardarbunga did not require the use of the sampler and thus it has not been tested in the field.

6. Digital cameras

Several digital cameras are in use by the mobile lab. Cameras capable of high speed imaging, time lapse, videos and normal SLR cameras. During the unrest and eruption of Bardarbunga these cameras proofed to be extremely useful to understand dynamic processes in case of lava emplacement. In the case of Bardarbunga event the area was fully covered by GSM-phone network thus images could be downloaded in near real time to the crisis centre.

Figure 5 Canon 1100d SLR camera. The advantage of digital imagery is that figures can be downloaded to the crisis center as soon as they have been taken.

7. GoPro video cameras

GoPro cameras are small and robust digital video cameras that can be used in a variety of environments. One of main problems during explosive eruptions is the fact that dust and water is abundant that can easily destroy delicate camera hardware. GoPro is designed forall weather conditions and they can withstand very harsh environments. Two GoPro cameras are in the arsenal of the mobile lab. These cameras are used to take time lapse photos in such a way that large areas can be covered. Repeated presence in same area can often reveal things that the human eye cannot.

Figure 6 The two GoPro cameras that the mobile lab uses extensively to monitor eruptions behavior.

II. Eruptions in Iceland: Best practice guidelines for aircraft observations

Magnús Tumi Gudmundsson, Þórdís Högnadóttir,Tobias Dürig
Nordvulk, Institute of Earth Sciences, University of Iceland

Halldór Björnsson
Icelandic Meteorological Office

Björn Oddsson
Department of Civil Protection and Emergency Management of the National Commissioner of the Icelandic Police

Version 2 – May 2015

Contents

Many volcanoes in Iceland are located in remote areas and visual ground-based observations of eruptions are in some cases sporadic and difficult. This applies in particular to eruptions within glaciers. Since the first air-based observations of a volcanic eruption in Vatnajökull to the north of Grímsvötn in 1938, aircraft has been used to a varying degree for eruption monitoring in Iceland. During the Gjálp eruption in 1996 and for all eruptions since, aircraft monitoring has been an important component of eruption response, particularly for events in glaciers.

Type of events to be expected:

- Explosive eruptions (phreatomagmatic, magmatic)
- Terrestrial effusive eruptions
- Subglacial/englacial eruptions
- Submarine to emergent eruptions
- Jökulhlaups, resulting from eruptions or drainage of geothermally-sustained cauldrons

These guidelines outline what is regarded as best practices for observations from aircraft of volcanic eruptions and volcano-related events. They are based on experience gathered over the last several years of observation in Iceland. The nature of response and observation depends on the nature of the activity, and therefore each type of event is covered separately. Documenting and reporting on inspection flights to civil protection authorities is covered at the end.

It is expected that this document will evolve with time as new methods of observation come into operation and new experience is gained. New updates will be numbered and dated; the current version is number 2, May 2015.

1 Preparation for flights, availability of aircraft, methods of observation, equipment

1.1 General considerations

The guidelines below do not take specific note of aircraft type and the equipment used for data gathering will depend on available options.

1.1.1 Common procedures and considerations

1.1.1.1 Communication with The Department of Civil Protection and Emergency Management of the National Commissioner of the Icelandic Police (NCIP-DCPEM) – Almannavarnadeild Ríkislögreglustjóra. On the basis of scientist's advice, NCIP-DCPEM takes decisions regarding inspection flights during crises, including arrangements needed for providing aircraft for flights.

1.1.1.2 What type of aircraft is available at that time

1.1.1.3 Personnel taking part in flight – determined strictly on basis of need – ensure competence for necessary data gathering and eruption assessment.

1.1.1.4 A scientist in charge is nominated for each flight. The scientist in charge is responsible for communication with pilot, and is responsible for flight observations according to these guidelines.

1.1.1.5 No-Fly Zone: Is the aircraft permitted to get into enough proximity of eruption to obtain useful data?

1.1.2 Consultation with pilots before flight

1.1.2.1 Where to go, what are the main targets and objectives of flight?

1.1.2.2 What type of monitoring equipment is on board and who will operate it

1.1.2.3 Where to place mobile monitoring equipments

1.1.2.4 Desired flying height

1.1.2.5 Weather conditions at volcano and en route

1.1.2.6 Information on wind direction and how to approach eruption site

1.1.2.7 Whether mobile phones may be used on the flight, means of communicating with civil protection and others if needed during flight.

1.1.2.8 Access to eruption site, No-Fly zone around volcano, is aircraft hampered by the zone

1.1.2.9 Get briefing from seismologists and hydrologists on what is currently known about eruption parameters

1.2 Aircraft

It depends a great deal on vent location, type of eruption, visibility and weather conditions which methods can be applied during inspection flights. The aircraft that have been used in recent years are:

1. Beech B200 Super King Air, two-engine aircraft. Owned by the Icelandic Civil Aviation Administration (ISAVIA). Used for regular monitoring of Katla. Equipped with ground clearance radar and DGPS for surface profiling. Especially valuable for monitoring ice surface changes in eruptions and other glacier-related events.
2. Dash 8, Icelandic Coast Guard. Equipped with SAR radar, Infrared cameras and long range visible cameras. Space to operate Laptop for on-board processing if needed.
3. Super Puma helicopters, Icelandic Coast Guard. Side door can be opened during flight for video, photography and FLIR.
4. Single-engine commercial aircraft, 4-6 seaters with windows that can be opened. Sometimes possible to take FLIR images through open windows.
5. Other, twin engine commercial aircraft, as available and when needed.

aircraft	run by	No. crew	No. scientists	range (km)	cruise speed (km/h)	on-board equipment	equipment to be brought by scientists	provided log files
Beechcraft Super King Air 200	ISAVIA	3	2-4	3338	536	DGPS, RADAR altimeter FIS[4]	GoPros, GPS	GPS, radar maps, IR images
Bombardier Dash 8Q-300	Icelandic Coastguard	4-5	4-12	4100	330 - 440	SAR[1], SLAR, EO-IR[2], MMS[3]	GoPros, GPS	GPS tracks, altimeter log
Eurocopter AS332 Super Puma	Icelandic Coastguard	5	6	840	252	EO-IR[5]	GoPros, GPS, handheld FLIR	GPS tracks, IR images[5]
Cessna 207A Skywagon	Eagle Air	1-2	2-4	1100	264		GoPros, GPS, handheld FLIR	GPS tracks (if available)

[1]Elta EL/M – 2022 (V) 3 maritime search radar [2]Wescam MX-15 gyro-stabilized EO-IR imaging system [3]Mission Management System [4]Flight Inspection System UNIFIS3000
[5]only some aircrafts

The following description of aircrafts and their range of application is based on the experiences of aircraft monitoring in the recent years.

1.2.1 Beechcraft 200 Super King Air (TF-FMS)

Owned by Icelandic Civil Aviation Administration (ISAVIA), this 2-engined aircraft has been used e.g. in surface profiling campaigns comprising regular glacier monitoring of Mýrdalsjökull (Katla) and Vatnajökull (e.g. Grímsvötn; Bárðarbunga). Equipped with a Flight Inspection System (FIS), a RADAR altimeter and differential GPS (DGPS), geo-referenced height profiles of the ground are obtained by flying low level along swaths over the region of interest. This mission profile requires favorable weather and viewing conditions. The ISAVIA crew usually consists of 3 persons (two pilots, one radar operator at the FIS). Depending on the seating configuration, 4-5 scientists can be additionally boarded. (For scientific surface profiling missions a minimum of 2 scientists is needed).

Three anchorage points have been shown to be most useful for attaching the GoPro cameras (see Figure 7): one camera in front view in the cockpit; and one for each side on the stern windows. While the front camera can be controlled via WiFi, the rear cameras are easily accessible from the rear seat, so they can swiftly switched on, replaced or relocated, when needed. Handheld GPS are best to be located close to the stern windows as well, but signal reception problems in other parts of the fuselage have not been observed for this plane.

Scratches and moisture at the windows can reduce the visibility. Due to the pressurized cabin, windows cannot be opened during a flight.

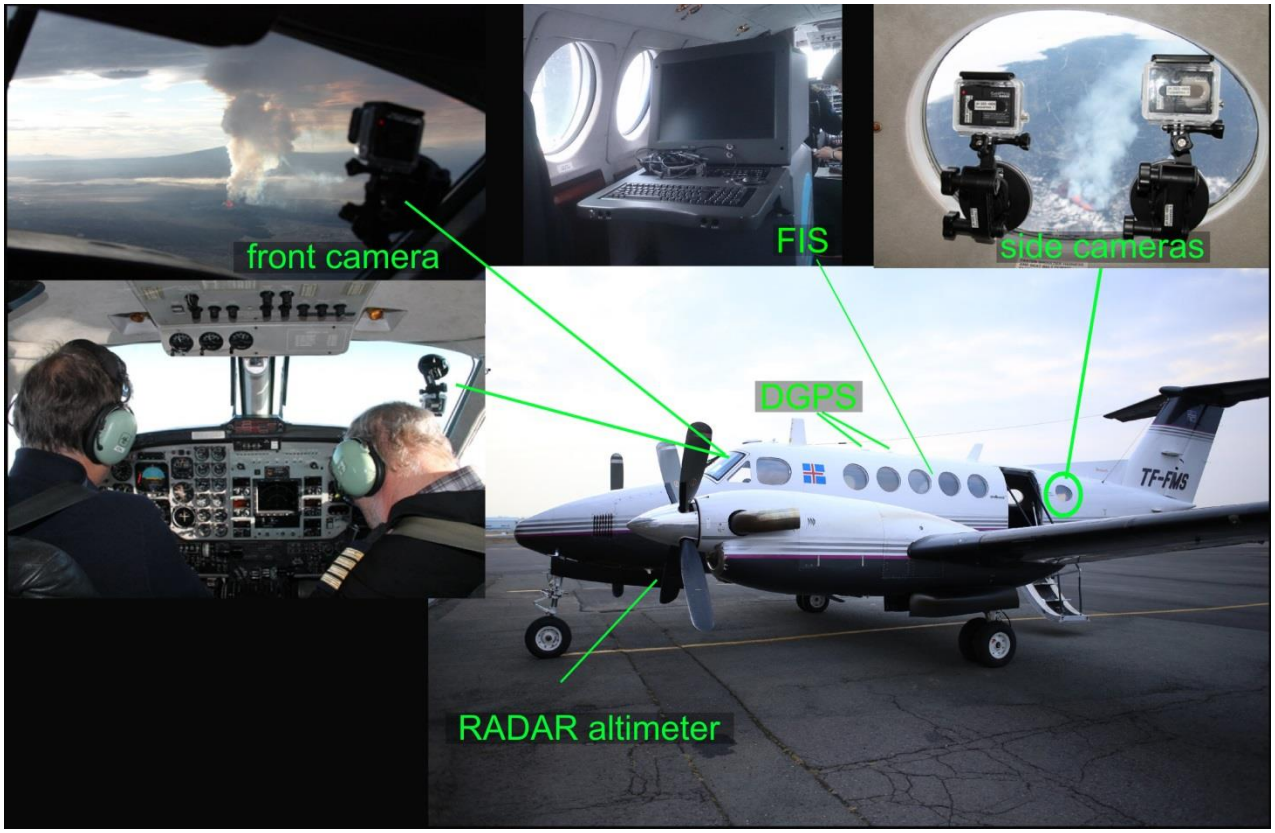

Figure 7. Monitoring equipment of the Beechcraft 200 flown by ISAVIA.

1.2.2 Bombardier Dash 8Q-300 (TF-SIF)

This 2-engined aircraft is run by the Icelandic Coast Guard and mainly used for maritime surveillance. Additionally it can be used for glacial inspection and eruption monitoring missions. The Dash 8 is equipped with a side looking airborne radar (SLAR), a 360° synthetic aperture radar (SAR) and a high resolution camera system that works both in the visible and infrared spectrum (EO-IR). This equipment allows surface scanning from remote locations at high altitudes regardless of the weather, which is an essential advantage for monitoring activities under unsettled Icelandic weather conditions.

The Coast Guard crew consists of 4-5 persons (2 pilots and 2-3 on the consoles, operating the Mission Management System). Up to 10 scientists can be boarded. Best locations for attaching the GoPro cameras are:

a) one camera in WiFi remote mode attached at the right cockpit window in front view
b) two cameras attached on both wide lookout stern windows. These cameras can be accessed easily.

Additionally handheld GPS devices should be used to guarantee that all pictures can be later georeferenced. The best location for the handheld GPS is close to a window, e.g. at the bottom of the lookout window as shown in Figure 8. The Dash 8 is equipped for long range missions, with sufficient space for scientists and crew to analyze large maps and use laptops.

Figure 8. Monitoring equipment of the Bombardier Dash 8, run by Icelandic Coast Guard.

1.2.3 Eurocopter AS332 Super Puma (TF-LIF, TF-GNA, TF-SYN)

These helicopters owned by Icelandic Coast Guard can carry up to 6 scientists, next to its 5 crew members. The side door can be opened during flight for video, photography and FLIR. Three anchorage points have been shown to be best for attaching the GoPro cameras (see Figure 9):

one forward (or sideward) looking camera mounted at the footboard of the helicopter and one for each side on the stern windows, where they can be easily accessed from the rear seat. The "outside" camera has to be remote controlled via WiFi. Crew and board team members should be warned not to hit the camera when stepping out. The handheld GPS devices should be attached close to the windows to guarantee sufficient satellite signal reception. Some helicopters are equipped with an onboard IR camera.

Figure 9. Eurocopter AS332 Super Puma (Icelandic Coast Guard) and suggested anchorage points for GoPro cameras.

1.2.4 Single-engined commercial aircraft (e.g. Cessna 207A Skywagon)

These smaller commercial aircrafts, usually 4-6 seaters, have the advantage that they might allow to open a window during flight, enabling a boarded scientist to take FLIR shots from a site. Attaching the GoPro cameras on such a plane should be in close consultation with the pilot. Typical locations for GoPro cameras is the cockpit front pane and/or the side windows (see Figure 10).

Figure 10. Cessna 207A Skywagon: Example for a single-engined commercial aircraft and suggested anchorage points for GoPro cameras. One of the windows can be opened during flight.

1.2.5 Two-engined commercial aircraft

Ask the pilot if a forward looking GoPro can be mounted in the cockpit. In this case use the WiFi remote control setting. GPS devices should be attached close to the windows or in the cockpit.

1.3 Other preparation and equipment

1.3.1 Reporting before flight

1.3.1.1 Notify NCIP-DCPEM and others who need to be notified of who is going and their mobile phone numbers.

1.3.1.2 Determine specific tasks of people going on flight.

1.3.2 Equipment list

1.3.2.1 Two hand-held GPS (e.g. Garmin 62). Should record position at 1 second interval throughout all parts of the flight where any data is gathered. In practice it is sensible to record the whole flight.

1.3.2.2 Three GoPro video recorders

1.3.2.3 Two EOS Canon cameras

1.3.2.4 Internal clocks of all cameras and video recording devices (GoPro, other video records, FLIR, etc.) need to be synchronized with the GPS at beginning of flight.

1.3.2.5 Spare batteries for GPS, cameras and video recorders.

1.3.2.6 Spare memory cards

1.3.2.7 Depending on aircraft, a laptop may be taken along, for downloading of data, and possible fast processing, e.g. for using Pixelcalc software for plume height determination.

1.3.2.8 Fieldbooks, pens, pencils, ruler etc.

1.3.2.9 Lists of contacts – telephone numbers of ground contacts

1.3.2.10 Short checklists on operation of cameras, video-recorders, GPS, how to synchronize clocks etc.

1.3.2.11 A folder and/or Pad/iPad:

- maps of all volcanic regions
- glacier bedrock and ice thickness maps
- geological maps
- Coordinate lists for previously defined eruption sites at volcanoes, central coordinates for volcanoes

2 Explosive eruptions

About 80% of all eruptions in Iceland are explosive or have a substantial explosive component. This is partly due to the high frequency of phreatomagmatic eruptions. These eruptions occur in glaciers (e.g. Grímsvötn, Katla) and where magma erupts through highly permeable and porous groundwater reservoirs or lakes (e.g. Laki, Eldgjá, Vatnaöldur, Veiðivötn). Many eruptions have both explosive and effusive components and some cause jökulhlaups An eruption with a substantial explosive component can be expected about once every 5 years in Iceland.

2.1 Observations – volcanological

2.1.1 Before flight

Get information from IMO, IES and NCIP- DCPEM on available information on expected eruption site, plume size and tephra fallout – see detail in 2.2.1.

2.1.2 During flight

*2.1.2.1 Vent location – determine accurate coordinates: **lat, long in degrees and minutes,** with elevation above sea level. Use any or all of the following methods: direct observation of vents, aircraft GPS, bearings to vent from different angles, SAR-images if flying in the Coast Guard Dash 8 (TF-SIF).*

2.1.2.2 Vent type (fissure, length of fissure, variations in activity along fissure, central vent etc.)

2.1.2.3 Plume height (in kilometers above sea level).

2.1.2.4 Direction of plume drift (in degrees from north)

2.1.2.5 Type of eruption (hawaiian, strombolian, vulcanian, sub-plinian, plinian, phreatomagmatic, subglacial)

2.1.2.6 Style of activity at vent (pulsating/continuous, if relevant: frequency of pluses, ballistics-heights reached by bombs, pyroclastic density currents observed, etc.)

2.1.2.7 Temperature of plume (using FLIR in a small aircraft, qualitative using TF-SIF thermal cameras).

*2.1.2.8 Plume colour (**white/grey/dark grey/black**)*

2.1.2.9 Fallout – distance from vent of visible fallout from plume (e.g. <1 km, 1-3 km, 3-10 km, 50 km, >100 km)

*2.1.2.10 Intensity of fallout - qualitative estimate based on observation of transparency of fallout blanket beneath main cloud/plume (e.g. give distance from vents in km where: **fallout blanket opaque / dark but some visibility / grey but transparent haze beneath cloud / traces of ash in air beneath cloud but visibility little affected**)*

2.1.2.11 Are there signs of lahar generation or conditions building up to lahars?

2.1.2.12 If lahar generation is considered possible, which areas/drainage sectors are most likely to be affected?

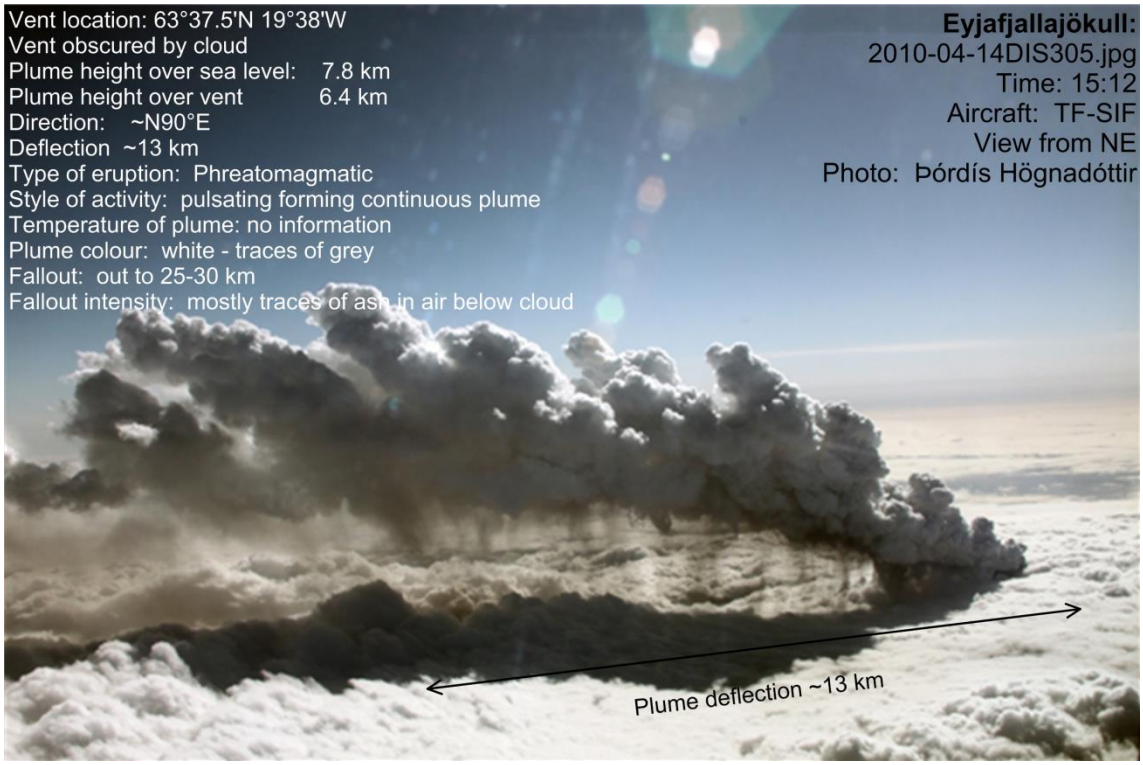

Figure 11. Example of aircraft observations: Plume during Eyjafjallajökull eruption on 14 April 2010. Listed is selected data obtained in flight, using available imagery and navigation tools.

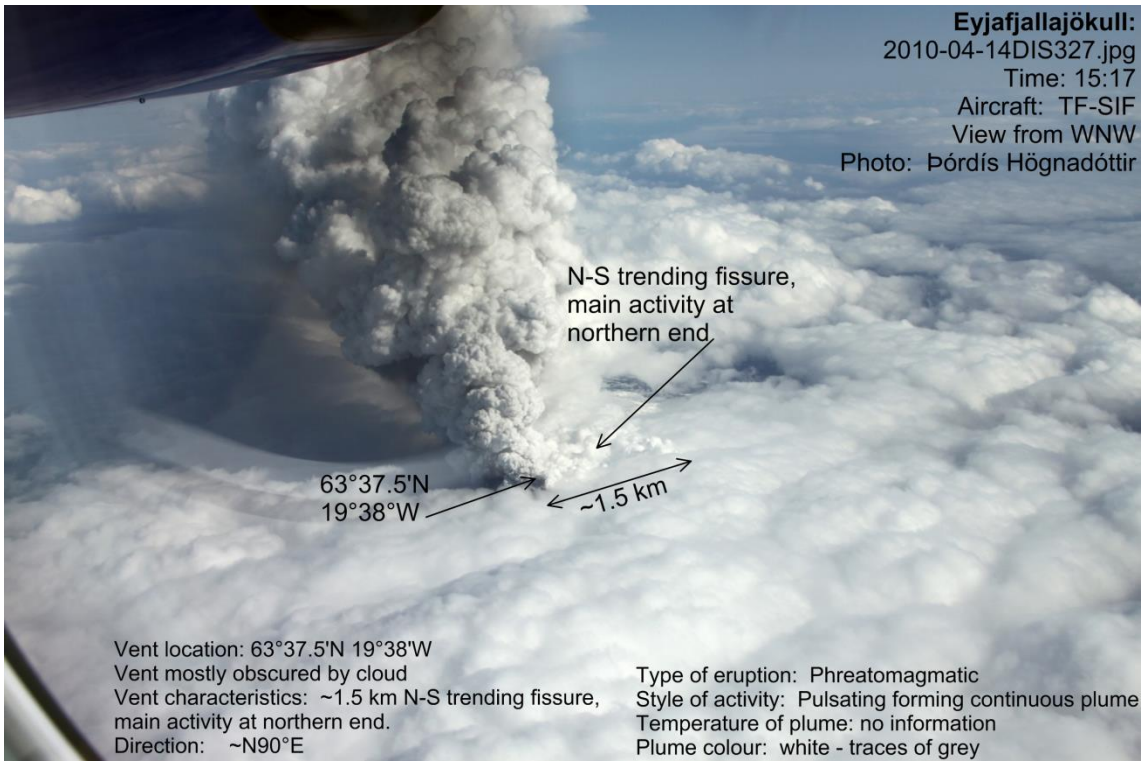

Figure 12. Example of aircraft observations: Vent area and plume (Eyjafjallajökull, 14 April 2010). Listed is selected data obtained in flight, using available imagery and navigation tools.

2.2 Observations – meteorological

2.2.1 Before flight

2.2.1.1 Is plume visible on radar?

2.2.1.2 Direction of plume drift if visible on radar

2.2.1.3 Plume height

2.2.1.4 Stability of plume over the last several hours

2.2.1.5 How does plume height compare with cloud top heights in vicinity of plume?

2.2.1.6 Latest information from sondes on atmospheric conditions

2.2.1.7 Plume information from MODIS/AVHRR/SEVIRI etc.

2.2.1.8 Ash retrievals from MODIS/AVHRR/SEVIRI

2.2.1.9 Lightning activity in the last 24 hours

2.2.1.10 Inspect wind-field at surface, 700 hPa (ca. FL100), 500 hPa (ca. FL170) and 300 hPa (FL300).

2.2.1.11 Get briefing of the status of eruption from seismologists, hydrologists or any other sources. Enter aircraft with an as complete picture of eruption and plume behavior as possible.

2.2.2 During flight (in addition to list for volcanological observations)

2.2.2.1 Height of clouds (cloud top height – of particular importance if plume not visible through clouds)

2.2.2.2 Velocity of plume drift (also direction of drift)

2.2.2.3 Wind speed – monitor changes with height with assistance from pilot

3 Terrestrial effusive eruptions

This type of eruption is common in ice free central volcanoes and on fissure swarms. None are exclusively effusive since fire fountaining usually provides a mild explosive component. This fire fountaining may at times lead to minor tephra fallout extending some kilometers from the vents. The frequency of these events is about one every 5-10 years.

3.1 Observations

3.1.1 Before flight

Same considerations as in 2.2.1 as needed

3.1.2 During flight

3.1.2.1 Vent location – determine accurate coordinates

3.1.2.2 Vent type (fissure, length of fissure, variations in activity along fissure, central vent etc.)

3.1.2.3 Extent and direction of lava flow progression

3.1.2.4 Area covered by lava

3.1.2.5 Estimate speed of progression of lava (by comparison with previous observations or time since start of eruption

3.1.2.6 Height of fire fountains

3.1.2.7 Height and location of crater walls

3.1.2.8 Plume generated from fire fountaining – height, colour, direction of drift (see explosive eruptions)

3.1.2.9 Fumes rising from lava (colour, areas where fumes visible)

3.1.2.10 Interaction of lava with environment (lakes, snow, ice etc.)

3.1.2.11 Are rootless cones and their formation observed?

4 Subglacial/englacial eruption

Subglacial eruptions are very common in Iceland; over 50% of all eruptions in Iceland occur in glaciers. Fully subglacial volcanic activity is usually confined to an early phase of each eruption. This phase is usually followed by an explosive phreatomagmatic eruption. In terms of hazards the subglacial eruptions are very potent and require observations over large areas, since meltwaters (jökulhlaups) usually emerge at the margin of the glacier that may be tens of kilometers away from the vents. This makes aircraft observations of particular importance. Eruptions of this type happen about once every 5-10 years.

4.1 Observations

Fundamental: Is eruption subglacial (fully under ice) or englacial (erupting through ice)?

4.1.1 Observations - Subglacial

4.1.1.1 Size of ice cauldrons/area where ice subsidence has taken place

4.1.1.2 Centre coordinates of ice cauldrons

4.1.1.3 Depth of ice cauldrons

4.1.1.4 Estimate volume of ice cauldrons

4.1.1.5 Look for evidence of disruption of ice outside obvious ice cauldrons – are there signs (crevasses, minor depressions) of new cauldrons forming?

4.1.1.6 Study pathway of meltwater – is there a depression marking the subglacial flowpath direction?

4.1.1.7 Are there crevasses on the expected flowpath indicating partial floatation of glacier – marking rapid propagation of a jökulhlaup?

4.1.1.8 Is a jökulhlaup currently emerging from the glacier or are there clear signs of a jökuhlaup?

4.1.2 Observations - Englacial

4.1.2.1 Determine all above as for a subglacial eruption (4.1.1).

4.1.2.2 Determine all as for an explosive eruption if a plume is present (2.1. and 2.2.).

4.1.2.3 Width of ice cauldrons with water level (usually bounded by sub-vertical ice walls)

4.1.2.4 Can water be seen in cauldrons?

4.1.2.5 Can craters be seen in cauldrons?

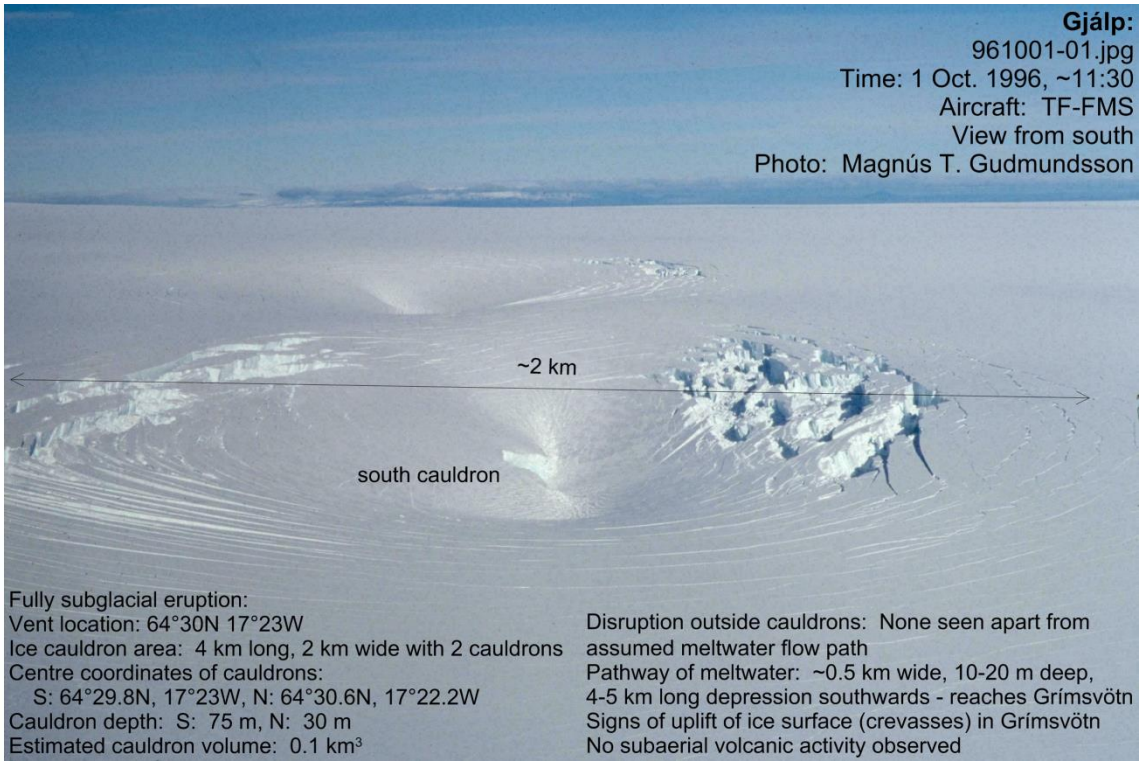

Figure 13. Example of observations over a fully subglacial eruption, the Gjálp eruption on 1 Oct. 1996. Listed is selected data obtained in flight, using available imagery and navigation tools.

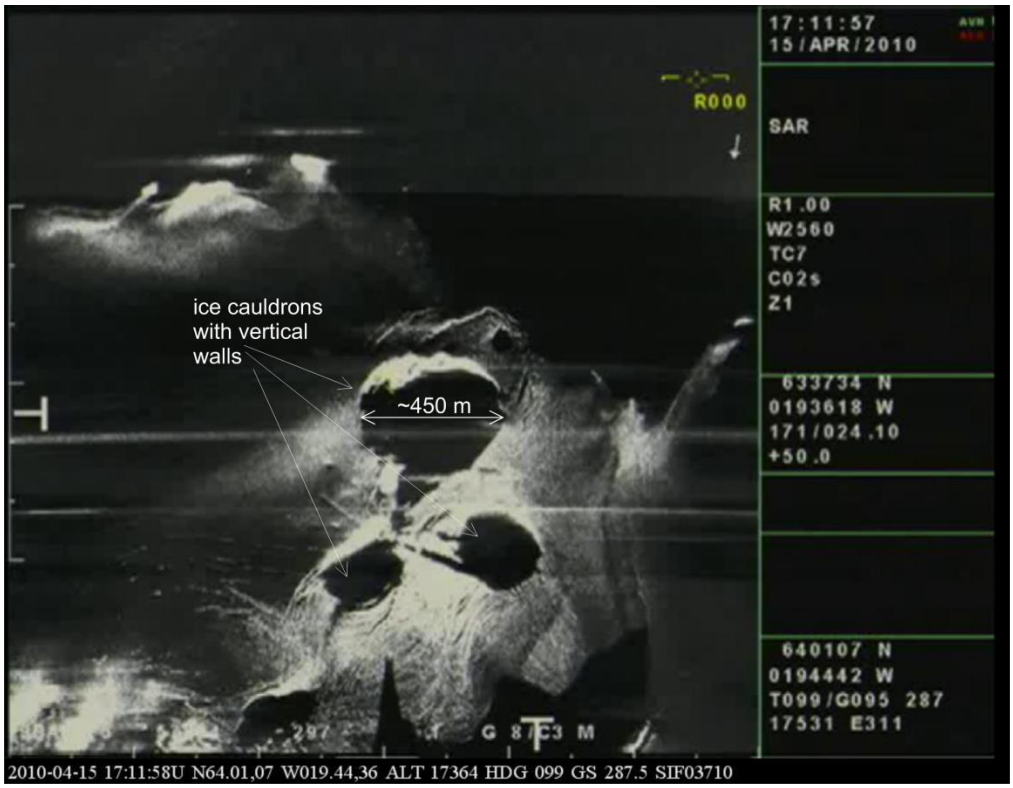

Figure 14. Example of observations with SAR radar on board TF-SIF. SAR-image of the summit of Eyjafjallajökull at 17:11:58 on 15 April 2010. Note ice cauldrons and crevasses.

5 Submarine to emergent eruptions

Events of this type can be expected on the Reykjanes Ridge, offshore Reykjanes, at the Vestmannaeyjar Archipelago, and offshore in the Tjörnes Fracture Zone and Kolbeinsey Ridge. The last confirmed events were the birth of Surtsey in 1963 and the northern end of the volcanic fissure in the Heimaey eruption in 1973.

5.1 Observations

5.1.1 Fully submerged

5.1.1.1 Signs of upwelling in ocean/lake surface

5.1.1.2 Is floating pumice observed? And if so, how large is the area of pumice?

5.1.1.3 Dead fish floating on surface?

5.1.2 Explosive

5.1.2.1 Determine as for 5.1.1 and for explosive eruptions (2.1 and 2.2).

5.1.2.2 Look for signs of submarine parts of active eruption, still fully submerged (5.1.1).

5.1.3 Emergent

5.1.3.1 Determine as for 5.1, 5.2, 2.1 and 2.2

5.1.3.2 Size of crater/emerging island

5.1.3.3 Height of island

5.1.3.4 Colour and apparent type of volcanic material making up island

5.1.3.5 If lava forming – extent of lavas

6 Jökulhlaups

The floods emerging from glaciers resulting from volcanic and geothermal activity are the most common type of volcanic hazard in Iceland, with a frequency of > one/year. Most of these are small events, not directly related to volcanic eruptions and usually do not cause damage. If there is uncertainty on source and other parameters, an inspection flight may be needed.

6.1 Observations

6.1.1 Within glacier

Identify source of jökulhlaup

Assuming a subglacial source – note that this list is very similar to the one on fully subglacial eruptions. It is also sometimes known only afterwards whether an event is associated with eruption of magma to the glacier bed or whether it is geothermal in character:

6.1.1.1 Size of ice cauldrons/area where ice subsidence has taken place

6.1.1.2 Centre coordinates of ice cauldrons

6.1.1.3 Depth of ice cauldrons

6.1.1.4 Estimate volume of ice cauldrons

6.1.1.5 Look for evidence of disruption of ice outside obvious ice cauldrons – are there signs (crevasses, minor depressions) of new cauldrons forming

6.1.1.6 Study pathway of meltwater – is there a depression marking the subglacial flowpath direction?

6.1.1.7 Are there crevasses on the expected flowpath indicating partial floatation of glacier – marking propagation of a jökulhlaup?

6.1.2 Flowpath outside glacier

6.1.2.1 Extent of jökuhlaup down river channel/floodpath

6.1.2.2 Width of jökulhlaup at one or more cross-sections

6.1.2.3 Is the jökulhlaup carrying ice blocks? And if so,

6.1.2.4 How big are the ice blocks?

6.1.2.5 How many ice blocks?

6.1.2.6 Is the jökulhlaup dilute (water flood), loaded with sediment (hyperconcentrated) or even a debris flow?

6.1.2.7 How fast is jökuhlaup propagating (if possible to observed jökuhlaup front).

6.1.2.8 Are there roads, power lines or dams in danger?

6.1.2.9 Are houses or inhabited areas in danger?

6.1.2.10 Are there people in the floodpath that need to be warned?

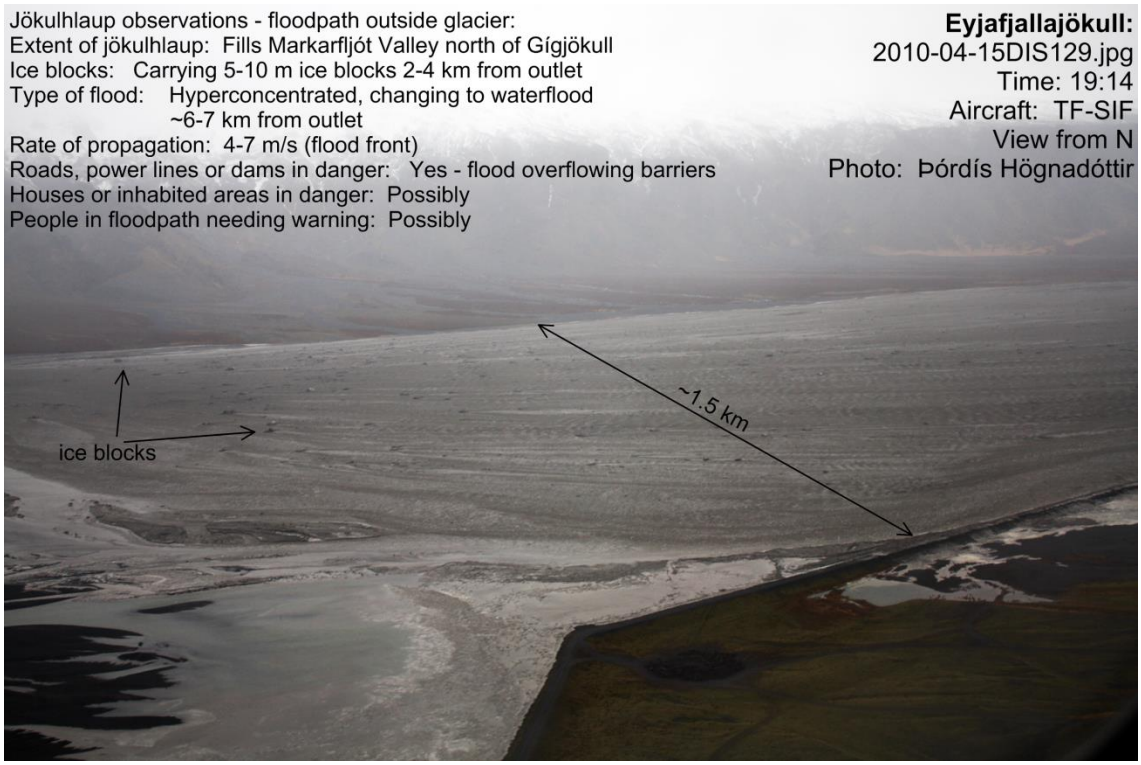

Figure 15. Aircraft observations of the jökulhlaup from Eyjafjallajökull on 15 April 2010. Listed is selected data obtained in flight, using available imagery and navigation tools.

7 When and how to inform and report to Civil Authorities

7.1 Prior to flight

7.1.1.1 Notify NCIP- DCPEM and others who need to be notified of who is going and their mobile phone numbers. What are the main tasks for the flight and what kind of information can be expected during and after the flight? Duration of flight and time of first expected information.

7.2 During flight

7.2.1.1 Notify NCIP- DCPEM of basic information when known (location, estimated magnitude, immediate hazards). If an imminent response to a hazard is to be taken, inform without delay. Use mobile phone if possible or communicate through aircraft radio.

7.2.1.2 During flight back to base (Reykjavík), prepare for briefing at NCIP- DCPEM. As possible estimate:

- ***source coordinates***
- ***eruption rate***
- ***plume height***
- ***direction of plume***
- ***area affected by tephra fallout***
- ***ice melting – cauldron size – magnitude of jökulhlaup***
- ***lava production***
- ***lava propagation rate***
- ***any thoughts on severity and hazard***

7.3 After flight

7.3.1.1 All scientific members of the flight report in person without delay to NCIP DCPEM to give a briefing on findings. Normally this would imply a meeting at NCIP DCPEM headquarters but it may happen through skype, phone or other comparable means if aircraft lands outside Reykjavík, e.g. in the case of airport closure due to tephra fallout.

7.3.1.2 A short memo is to be produced for each flight. This memo should mostly be filled out during flight but finalized after flight. The memo should include:

- Date, time, aircraft, pilots, participants
- Reason for flight
- List of equipment used
- List of data gathered (e.g. photos, video, infrared images, infrared video, etc.)
- Short summary of findings during flight – using numbered headings in line with these guidelines.
- Overall assessment if considered needed in addition to items above.

Appendix II-A: Checklist prior to flight

Garmins (GPS)

switch on GPS			
check battery status ➢ if less than 2 bars: change batteries!			
wait for satellite signal*			

*Note: if indoors, position GPS very close to a window!

➢ use now GPS clock for synchronization (see subsequent procedures)

Canon 1 & Canon 2

switch on Canon camera		
check battery status ➢ if less than 2 bars: change batteries!		
push "menu" button, go to time settings		
select minutes and seconds slightly prior to GPS time*		
in the instant when GPS displays pre-selected time: ➢ activate camera time by selecting "OK"		
check if camera time is now synchronized to the second ➢ if not: repeat synchronization procedure		
switch off Canon camera		

*Note: In this stage the camera time is halted!

GoPro 1, GoPro 2 & GoPro 5

adjust LCD display			
switch on GoPro (by using front button)			
➢ if "one button mode" is activated: hold top (trigger) button pressed until recording is stopped			
use front button and top button to get into "date & time" menu			
select minute slightly prior to GPS time			
wait until GPS clock turns to the respective minute, activate camera time by selecting "OK"			
take photo or movie (length > 3s) of GPS clock			

switch off GoPro by holding front button pressed			

Final checks

switch off Garmins			
store Garmins			
store GoPros and GoPro cases			
check and store complementary GoPro gears			
store replacement batteries for Garmins			
store replacement batteries for GoPros			
store replacement batteries for Canons			
print and store relevant maps			
store gas masks			
store replacement filters for gas masks			
store gas sensor			
inform IES about estimated departure and arrival time			

Appendix II-B: Credits

Figure	Photo taken by
7	Ingi Bjarnason, Magnús T. Gudmundsson, Stéphanie Dumont, Tobias Dürig
8	Magnús T. Gudmundsson, Tobias Dürig, Ásta Rut Hjartardóttir, Þórdís Högnadóttir, Freysteinn Sigmundsson
9	Tobias Dürig
10	Tobias Dürig, Stéphanie Dumont, Ashley Davies
11	Þórdís Högnadóttir
12	Þórdís Högnadóttir
13	Magnús T. Gudmundsson
14	
15	Þórdís Högnadóttir

III. Eyjafjallajökull eruption of 2010: Comparison of plume model predictions with observed fallout

Tobias Dürig, Magnús T. Gudmundsson, Thorbjörg Ágústsdóttir[1], Thórdís Högnadóttir.

Nordvulk, Institute of Earth Sciences, University of Iceland.

1: Present address: Bullard Labs., Dept. of Earth Sciences, University of Cambridge

Introduction

The eruption of Eyjafjallajökull in 2010 provided a wealth of data on explosive activity. It displayed considerable variety in plume strength with plume heights generally in the range 4-10 km over sea level (Arason et al., 2011; Gudmundsson et al., 2012). The plume of Eyjafjallajökull for most of the eruption classifies as weak or bent-over (Sparks et al., 1997). It has been suggested that its height was considerably reduced by the wind, and that simple plume models linking plume height with magma discharge, either based directly on Morton et al. (1956) theoretical model, or empirical data fitting (Sparks et al., 1997; Mastin et al., 2009) underestimate greatly the mass discharge rate (Bursik et al., 2012; Woodhouse et al., 2012). This issue can be studied further by comparing model predictions on mass erupted with the amount of mass deposited as tephra, since fallout was measured in considerable detail at about 400 locations in Iceland (Gudmundsson et al., 2012). For the part of the tephra that fell into the ocean south and southeast of Iceland a considerable uncertainty exists, but the magnitude of this component can nevertheless be estimated using well established behaviour of tephra layers of thinning with distance (e.g. Thorarinsson, 1954, Pyle, 1989; Fierstein and Nathenson, 1992). In this report data on plume height are used to estimate predicted mass discharge for individual phases of the Eyjafjallajökull eruption using several published models. The results are compared with the measurements of fallout obtained in 2010 and the performance of different models assessed. However, before this comparison is made, the plume height data, obtained from C-band radar in Keflavík, 155 km to the WNW of the volcano is assessed. A set of 105 height determinations from photographs of the plume, mainly obtained in inspection flights, is used to calibrate the radar plume height data. Moreover, these aircraft data are used to estimate the deflection of the plume as a function of wind speed at 5 km height. A simple linear best fit linking these parameters is obtained.

The Eyjafjallajökull eruption

Sustained explosive activity was observed for 39 days during the eruption of Eyjafjallajökull in 2010 (e.g. Gudmundsson et al., 2012). Activity ranged from predominantly phreatomagmatic early in the eruption progressing later to dry magmatic fragmentation (Dellino et al., 2012). The four main phases following the few hour long initial subglacial phase (Gudmundsson et al., 2012) were the first explosive phase ("phase I", 14-18 April), the low-discharge effusive phase ("phase II", 18 April-4 May) with relatively weak but sustained explosive activity, the second explosive phase ("phase III", 5 -17 May), and the final phase ("phase IV", 18-22 May).

Data

The data used in this study are:

i) Plume height obtained by the Icelandic Meteorological Office (IMO) from the C-band radar in Keflavík (Arason et al., 2011).
ii) Plume height as measured from photographs taken on board an inspection aircraft.
iii) Plume height as measured from the ground using triangulation or photographs.
iv) Wind speed and direction at approximately 5 km altitude is retrieved from the operational analysis of the European Centre for Medium Weather Forecasts (ECMWF).

An additional set of data exists on plume height, the photos from web-cams on ground to the north and northwest of Eyjafjallajökull (Björnsson et al., 2013). These data are not used here. However, the plume deflection correction derived below provides a tool to correct plume heights obtained from the web cams. This is because the deflection was principally towards south to southeast while the web cams are located to the north and west-northwest of the volcano. Using the distance to vent from the web-cams therefore leads to underestimates in plume height, since the plume top was located some kilometers further away.

Radar data

The C-band radar at Keflavík airport was the only weather radar operating in Iceland at the time of the eruption. The sampling strategy of the radar was to scan at vertical angles of 0.5°, 0.9°, 1.3°, 2.4°, 3.5°, 4.5° and 6° (Arason et al., 2011). The width of the beam is 0.9° providing some overlap between scans. At a the distance of Eyjafjallajökull the vertical distance between the beams of the lowest scanning angles is about 1.1 km and about 3 km between 1.3° and 2.4°. This leads to steps in the plume heights obtained from the radar, with preferential sampling at about 2.7, 3.9, 5.0 and ~8 km height for a target 155 km away. This limits to some extent the accuracy of the data obtained from the Keflavík C-band radar (for details see Arason et al., 2011, see also Oddsson et al., 2012).

The radar scans the horizon once every 5 minutes. Thus, at times when the plume was not below the visible horizon from Keflavík, which limits the lowest observable plume to 2.9 km, the plume can be detected provided it is not obscured within cloud. The data can also be combined into e.g. median and average values over 3 or 6 hour long periods.

Photos

Monitoring of vent activity and visual observations of early plume behaviour took place in inspection flights (see complete list of inspection flights in Appendix. 6.2 in Thorkelsson (ed.), 2012, http://www.vedur.is/media/ICAOreport_web_lr.pdf). For most of these flights the aircraft location was recorded with GPS (Figure 16), and through linking camera clocks with the GPS, location of aircraft at time of photography could be determined. This linking process involved determining the asimuth of several photos from each flight and in that way correcting for shifts in camera clocks. This was necessary since the process of syncronizing camera clock and GPS had not been implemented for inspection flights in 2010. The camera azimuth-flight path linking provides in general an accuracy of about 1 km in camera location. This is therefore the maximum error in the distance between aircraft and the volcanic vents, or any other reasonably well defined target.

The height of plume is calculated using the software Pixelcalc (Magnússon, 2012) – written in Python to obtain heights and other distances from digital photos, using picture

metadata to derive lens and camera specifics to convert distances on photo to actual lengths at the location of the target, given a known camera-target distance. The software corrects for earth's curvature at distances where it becomes significant. In most cases the plume height is obtained by measuring the distance between the plume top and the land underneath, taking into account plume deflection by wind and land height under the plume top to obtain the height above sea level. In some cases height over clouds is determined. However, such observations are only used where an independent measurement of cloud top height is available. Such cloud heights are in some cases obtained by direct observation using aircraft altimeter or through independent cloud height measurement using Pixelcalc. The Pixelcalc heights are considered to have an uncertainty of not more than 0.5 km.

Photographs taken on the ground are used in some cases. For these the location of the camera is accurately known and therefore distance to plume top can be calculated. Independent information of plume azimuth is used to correct for plume top deflection relative to vents.

The total number of photos taken on inspection flights is counted in thousands. Not all flights provided photos that allow reliable determination of plume height, due to e.g. cloud cover, flight route and sometimes difficulties in getting into suitable range of the plume. Only the photos best suited for analysis were used, yielding in total 77 data pairs radar-photo of plume heights.

Wind speed at 5 km elevation

The records from the operational analysis of the European Centre for Medium Weather Forecasts (ECMWF) were obtained through the IMO. These data are proved as tables of wind speed at 300 hPa, 500 hPa (~5 km height) for a specific location every 6 hours.

Web-cam data

A large set of photos exists from web cams at Hvolsvöllur (33 km WNW from vents) and Þórólfsfell (9 km N from vents). These data are not used here but they are described by Arason et al. (2011).

Methods

The key parameter for plume models used to estimate the mass flux in a volcanic eruption is the plume height. These models are either based on buoyancy theory (Morton et al., 1956) or empirical correlations between plume height during eruption and the quantity of tephra deposits formed (Sparks et al., 1997; Mastin et al., 2009). Recently the effect of wind on weak plumes has been explored, leading to new, more complicated models linking atmospheric parameters with plume height and the derived mass eruption rate (Woodhouse et al., 2013; Degruyter and Bonadonna, 2012). The models (Eq. 1-4) are presented in such a way that the input is plume height *h* in meters and the output is mass eruption rate (MER) in kg/s. In addition, the models applied here are for simplicity named by their first authors and referred to as:

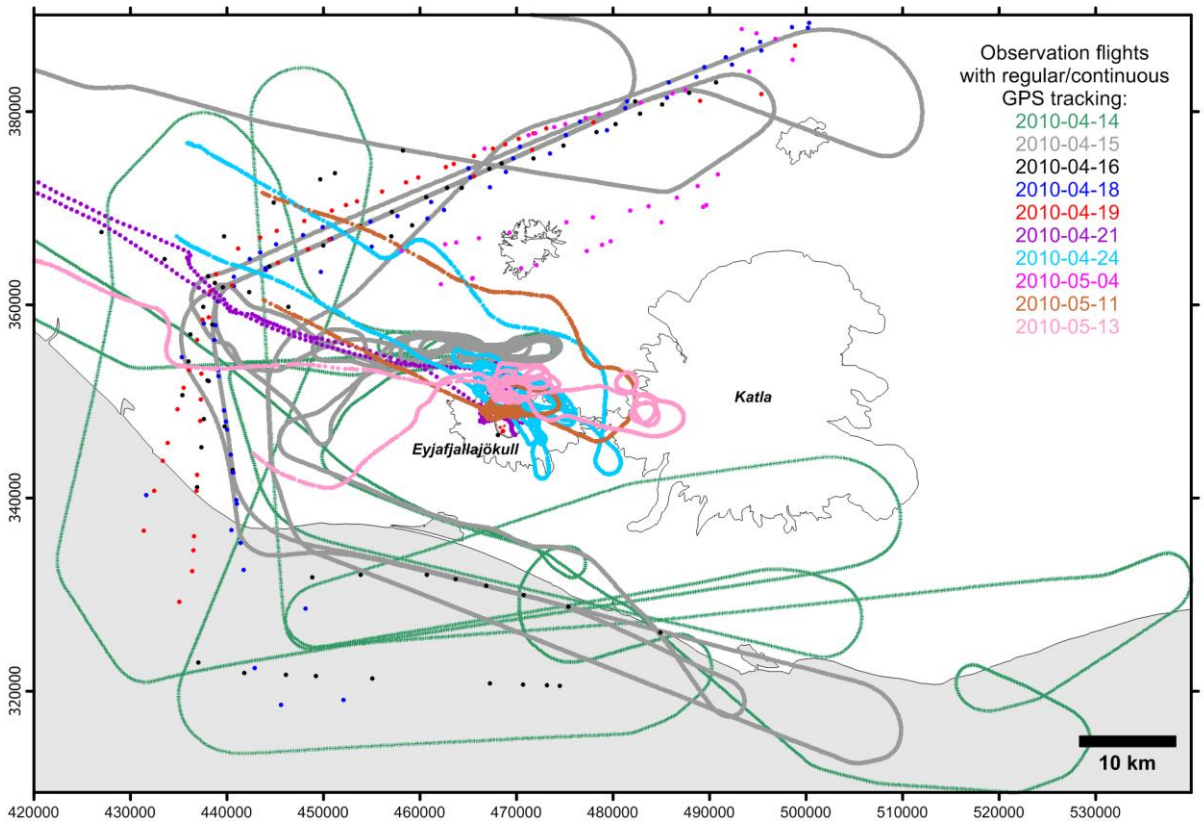

Figure 16. Flight paths of observation flights during the Eyjafjallajökull eruption in April-May 2010, where regularly sampled GPS coordinates exist. Photos were taken on all of these flights as well as several that were taken on the ground at various dates.

- "Wilson" (Wilson and Walker, 1987) - a theoretical model which estimates the mass flux *Q* by:

$$Q_{Wilson} = (h/c)^4 \quad (1)$$

where *h* denotes the plume height (in m) and *c* is a constant which is 236m(s/kg)$^{1/4}$.

- "Sparks" (Sparks et al., 1997) - an empirical model which approximates *Q* by:

$$Q_{Sparks} = \rho \cdot (h/c)^{3.86} \quad (2)$$

where ρ is the DRE of the magma erupted and forming the plume, and *c* is 1670m(s/m^3)$^{1/3.86}$.

- "Mastin" (Mastin et al., 2009) – an empirical model which estimates the mass flux by:

$$Q_{Mastin} = \rho \cdot (h/c)^{4.15} \quad (3)$$

where *c* is given by 2000m(s/m^3)$^{1/4.15}$.

- "Woodhouse" (Woodhouse et al., 2013) – a theoretical model which estimates the mass flux by:

$$Q_{Woodhouse} = \pi \cdot \left(\frac{h}{318} \cdot \frac{1+4.266 \cdot u+0.3527 \cdot u^2}{1+1.373 \cdot u}\right)^{3.95} \quad (4)$$

with $u = 1.44 \cdot w/(NH_1)$ where w is the wind speed at height H_1 and N the buoyancy frequency, which can be taken as $0.01 s^{-1}$ for the Eyjafjallajökull 2010 eruption. Additionally, 3 variants of the "Wilson" model were tested which use Eq. (1), but with different constants c basing on empirical results on plumes with basaltic tephra. They are referred to as:

- "Wehrmann" (Wehrmann et al., 2006) which uses $295 m(s/kg)^{1/4}$ for c.
- "Scollo" (Scollo et al., 2007) for which $247 m(s/kg)^{1/4}$ is selected for c.
- "Andronico" (Andronico et al., 2008) which uses $244 m(s/kg)^{1/4}$ for c.

In Figure 17 the plume heights obtained by both methods are displayed for the total period of the eruption. Based on the comparison of the 77 data pairs, it turned out that in average, photo-based plume heights are 0.5 km higher (see Figures 17 and 18). As a first step for data quality improvement, this systematic shift was corrected by adding this value to all radar-derived plume heights.

The radar data set based on 5 minutes sampling intervals suffers from the fact that it is incomplete (Arason et al., 2011). In order to use a data set with a better coverage over the complete period of eruption, the time intervals of plume height assessment have to be increased. In order to study the consequences of this data reduction, 42 six-hour intervals were selected for which the radar data sets provide the best coverage (containing at least 60 of 72 data points measured at 5 minutes intervals). These 42 data sets were obtained in phase I (7 data sets) and phase III (35 data sets) of the eruption.

Using empirical plume height models, the predicted mass M_i erupted for each of these 6h periods was computed, based on:

I. 5 minutes radar height data h_{5min} referred to as "5min data"
II. mean, median and maximum heights (h_{3h_avg}, h_{3h_med}, h_{3h_max}) within two 3h intervals referred to as "3h data"
III. mean, median and maximum heights (h_{6h_avg}, h_{6h_med}, h_{6h_max}) within the 6h interval, referred to as "6h data"

For the 5 minutes time resolution, the integrated mass M_{i_5min} over a 6h interval was calculated by:

$$M_{i\_5min} = \sum_{j=1}^{72} Q_{j,model}(h_{5min,j}) \cdot \Delta t \quad (5)$$

with the time interval Δt = 300s and $Q_{j,model}(h_{5min,j})$ being the mass flux Q_j provided by a specific model with $h_{5min,j}$ as input parameter.

Missing data points within the 5min data set were assigned to the average height value within the 6h interval. (For example, if 12 of 72 data points were missing, the integrated mass was scaled up by a factor of 72/60).

For the 3h data, the integrated mass M_{i_3h} over a 6h interval was quantified by:

$$M_{i\_3h} = \sum_{j=1}^{2} Q_{j,model}(h_{3h,j}) \cdot \Delta t \quad (6)$$

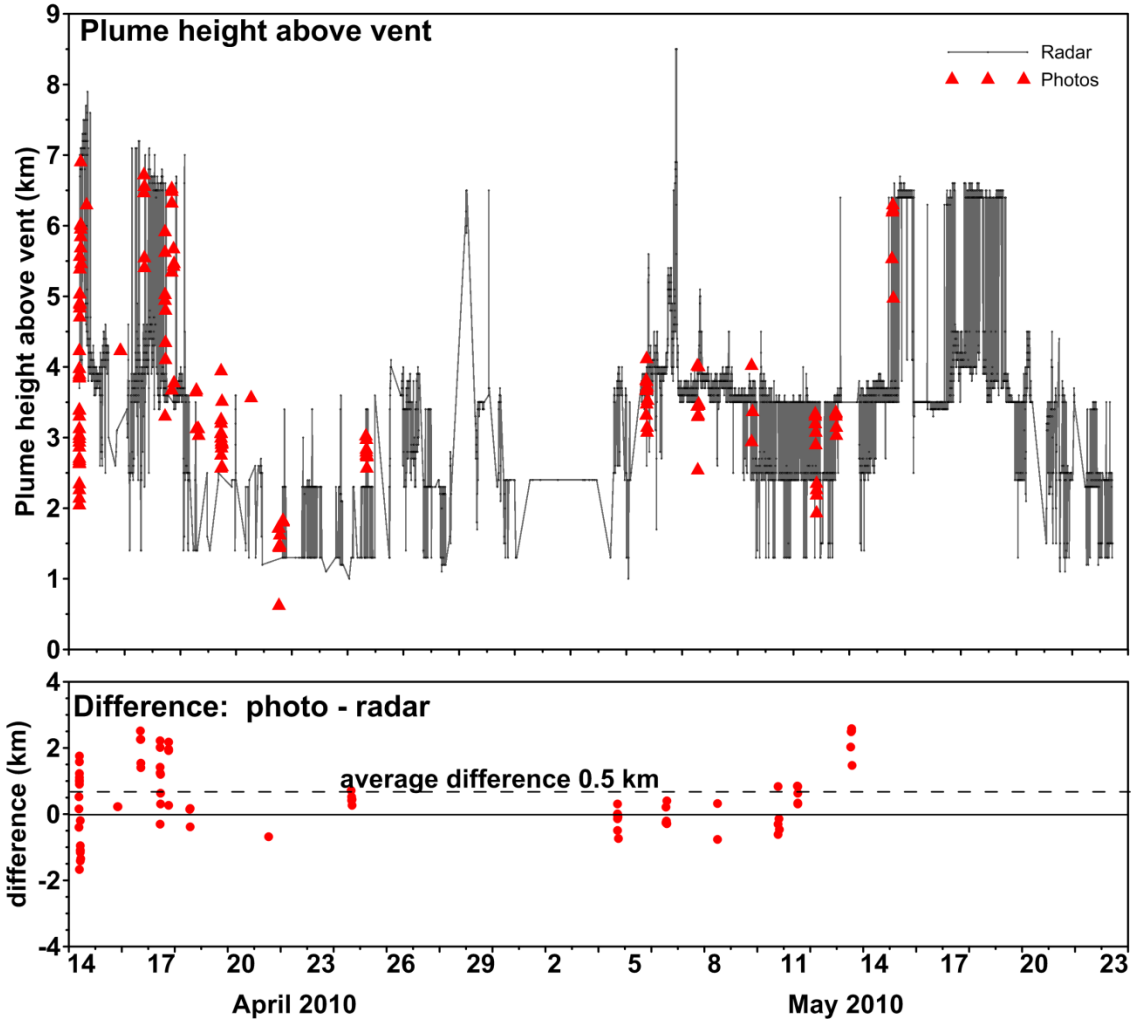

Figure 17. Top: Plume height from the Keflavík C-band radar and photographs during the Eyjafjallajökull eruption. Bottom: Difference between the two methods. The large scatter in the difference is largely due to the stepping in the radar plume height.

with Δt = 10800s (= 3h) and $h_{3h,j}$ being h_{3h_avg}, h_{3h_med}, h_{3h_max}, i.e. the mean, median or maximum value of the 3h interval number j within the 6h interval observed.

The accumulated mass M_{i_6h} over a 6h interval was computed by:

$$M_{i\_6h} = Q_{model}(h_{6h}) \cdot \Delta t \qquad (7)$$

with Δt = 21600s (= 6h) and h_{6h} being h_{6h_avg}, h_{6h_med} or h_{6h_max}, depending on the procedure tested.

Using three models (Wilson, Mastin, Sparks), two time intervals (3h, 6h) and three statistical operations (mean, median and maximum) result hence in 18 different estimates of M_i for each of the i=42 analyzed 6h intervals, which are compared to the respective value M_{i_5min} based on the 5 minute data sets, by generating the ratio Y:

$$Y_i = M_i / M_{i\_5min} \qquad (8)$$

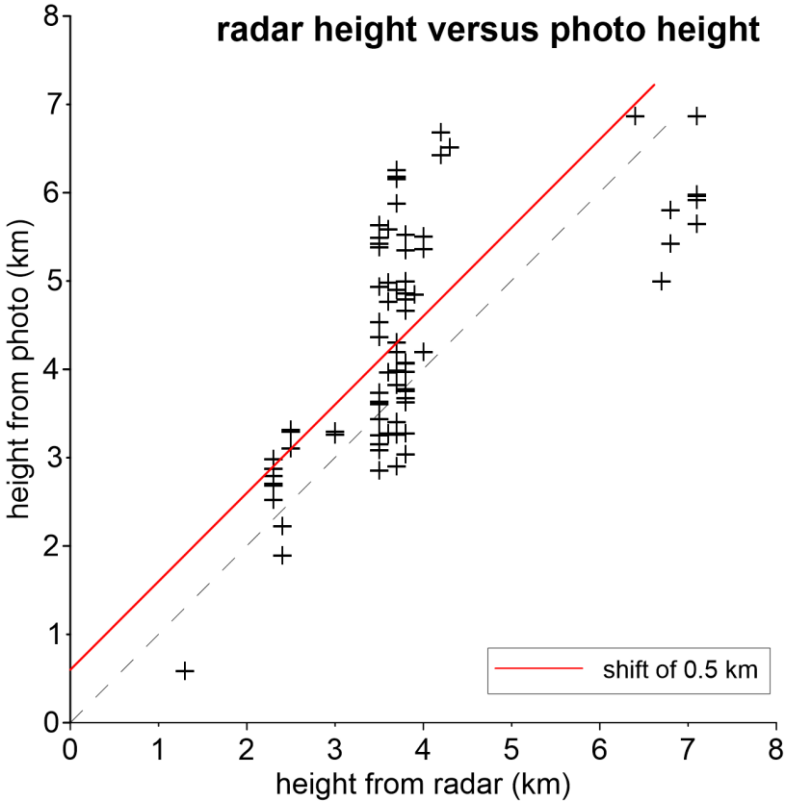

Figure 18. Radar-derived heights and photo-derived heights of plume relative to vent (vent height 1.5 km a.s.l.).

The ratio *Y* can be treated as a quality factor: In the best case *Y* is 1, meaning that the way being tested to estimate the mass and the mass based on the original five minute data set are equal. The larger the deviation from *Y* to 1, the less reliable is the method of approximation.

Based on the findings of these multivariate comparative analysis it is possible to find the optimum compromise between data coverage and data quality. Once the best procedure and time interval is found, 1/*Y* can be used as a correction factor for the reduced data.

By applying this method, a comprehensive data set with a good coverage was constructed for the whole eruption which serves as a robust base to calculate the model-predicted mass erupted within the chosen time interval Δt using the set of plume height models presented above.

In order to check the capability of these models in reproducing mass eruption rates, the individual model-derived results for the four main stages of the eruption were finally compared to the total masses obtained for each of the four phases, based on the mapped fallout and exponential dispersal models for the offshore part (Gudmundsson et al. 2012).

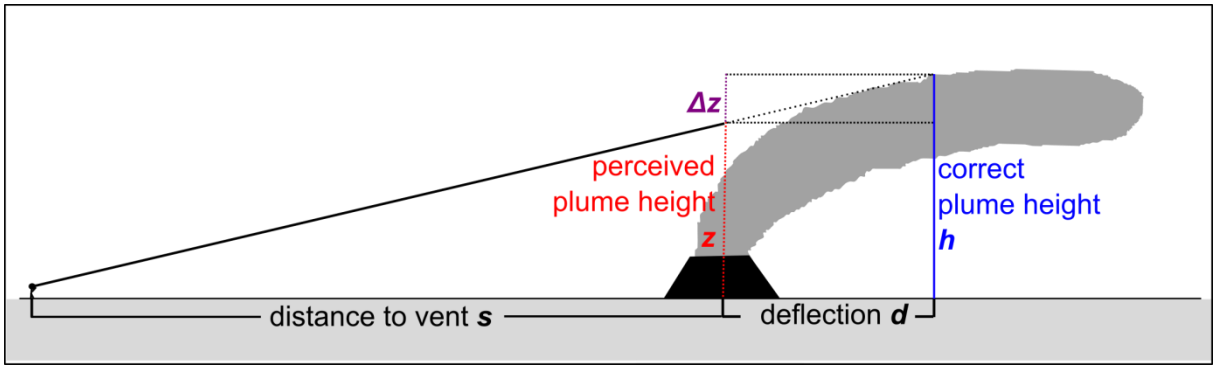

Figure 19. Effects of plume deflection on plume height calculation. In cases where plume is deflected away from observation point (camera) the true distance to plume top will be greater than the distance to the vent.

Results

Wind effects on ash plume - Horizontal deflection

For plume height measurements using photos and web cameras it is of particular importance to consider the potential effects of horizontal deflection, which can cause an underestimate of the actual plume height (see Figure 19).

The larger the deflection and the closer the observer is to the vent, the larger the error due to the increasing difference *Δz* between the wrongly perceived plume height *z* (location of the plume top over vent) and correct maximum plume height *h*.

The deflection shows considerable scatter, but to a first order during the 2010 Eyjafjallajökull eruption, the horizontal deflection *d* is shown to be linearly correlated to the wind speed (Figure 20).

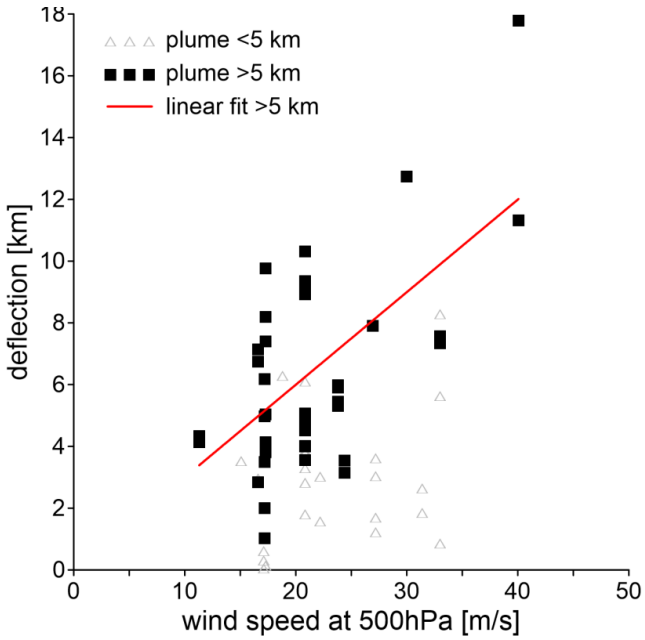

Figure 20: Horizontal distance from vent to plume top in the Eyjafjallajökull eruption as afunction of wind speed at 500hPa (~5 km a.s.l.). Only plume heights of 5km or more are used in the correlation.

In Figure 20, the horizontal deflection (obtained by photogrammetry) is plotted versus the wind speed at 500hPa, which gives the wind field velocities at an altitude of approx. 5km a.s.l. The data points which are attributed to a plume height of >5km (marked by black squares) show a clear linear trend, described by the function

$$d = a \cdot w \tag{9}$$

where *d* is the horizontal deflection (in m), *w* the wind speed at 500hPa and *a* is a characteristic parameter with the dimension of time. In the case of Eyjafjallajökull 2010, we find the value of *a* being ~300s.

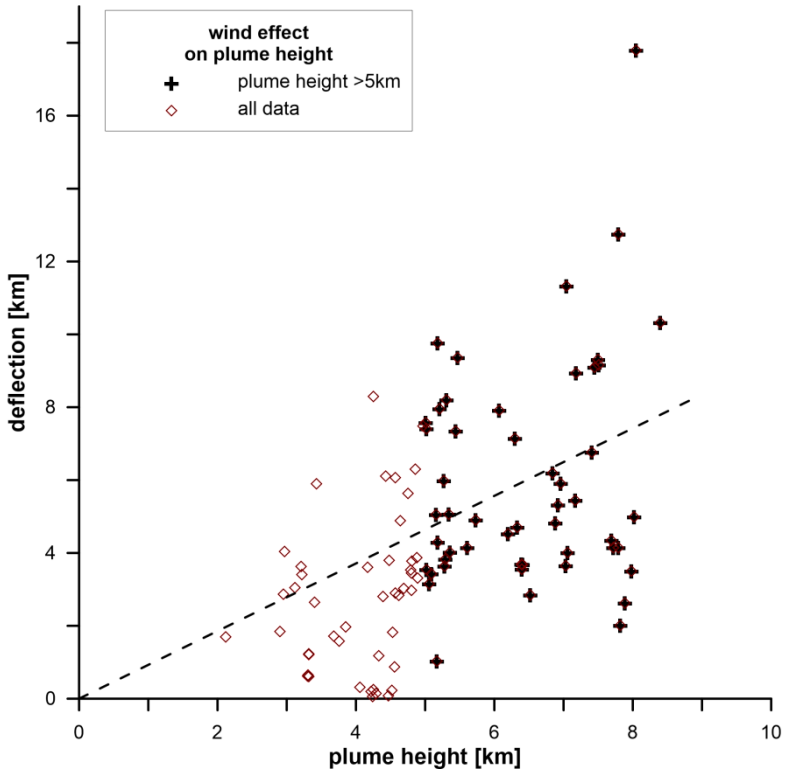

Figure 21. Correlation between plume height and horizontal plume deflection.

Wind effect on plume height

While the deflection does not affect the accuracy of radar based data, another wind effect has to be considered for all methods that depend on plume heights as input parameter, which is the wind-related plume height reduction. Plume modelers are well aware of this effect and current numerical models (e.g. Degruyter and Bonadonna, 2012; Woodhouse et al., 2013) are developed with the aim of taking this effect into account. Although general conclusions cannot be obtained from this graph, the data for Eyjafjallajökull indicate a correlation between deflection and plume height (Figure 21).

Bridging the radar data gaps – effect of time intervals on modelled mass flux values

Table 1 presents the resulting values of the ratio *Y* calculated by Eq. (8) for all 18 configurations tested. Based on these results it can be stated that for the 3h and 6h time intervals:

1. Maximum plume heights: All models tested show large values for *Y* (meaning a large overestimate relative to the 5 minute data set used as benchmark) and a significant scatter (large standard deviations).
2. Mean and median heights: All models and for both time intervals give *Y* values close to 0.9.
3. The Y values for median plume heights show a larger scatter than the mean heights. This might be an effect of the stepped nature of the radar scan technique used.
4. The difference between using mean values of plume heights for 3h intervals versus 6h intervals does not significantly affect the output quality: The Y values remain similar.

Table 1: Comparison of 3h and 6h radar data with 5 minute data.

Table 1: *Y*			N	average			median			maximum		
				Wilson	Mastin	Sparks	Wilson	Mastin	Sparks	Wilson	Mastin	Sparks
3h	phase I	mean	7	0.82	0.81	0.83	0.80	0.79	0.81	2.89	2.99	2.80
		st dev		*0.09*	*0.10*	*0.08*	*0.20*	*0.21*	*0.20*	*1.43*	*1.55*	*1.33*
	phase III	mean	35	0.91	0.91	0.92	0.91	0.91	0.92	1.85	1.90	1.81
		st dev		*0.10*	*0.10*	*0.09*	*0.24*	*0.25*	*0.23*	*0.95*	*1.01*	*0.90*
	total	mean	**42**	**0.90**	**0.89**	**0.91**	**0.90**	**0.89**	**0.90**	**2.03**	**2.08**	**1.98**
6h	phase I	mean	7	0.80	0.79	0.82	0.73	1.01	0.76	4.02	5.97	3.90
		st dev		*0.10*	*0.11*	*0.09*	*0.27*	*0.36*	*0.28*	*2.98*	*4.51*	*2.84*
	phase III	mean	35	0.90	0.90	0.91	0.93	0.92	0.93	2.40	2.48	2.33
		st dev		*0.11*	*0.12*	*0.10*	*0.28*	*0.29*	*0.27*	*1.84*	*1.97*	*1.72*
	total	mean	**42**	**0.89**	**0.88**	**0.89**	**0.89**	**0.94**	**0.90**	**2.67**	**3.06**	**2.59**

Thus, the best balance between data coverage and output accuracy of mass flux models is ensured by using the mean values of recorded plume heights on a 6h time base. According to the results for Eyjafjallajökull 2010 this procedure leads to slight underestimates of mass fluxes with the 6h model values giving respectively 88%, 89% and 89% of the 5 min values for the Mastin, Wilson and Sparks models. Mass eruption rates based on such input data should therefore to be corrected by scaling the output with the factor of 1/0.89 (= 1.12).

For illustration, Figure 22 shows original and corrected mass eruption rates computed by the three models presented in Table 1 for phase III of the eruption (between 5 and 17 May 2010).

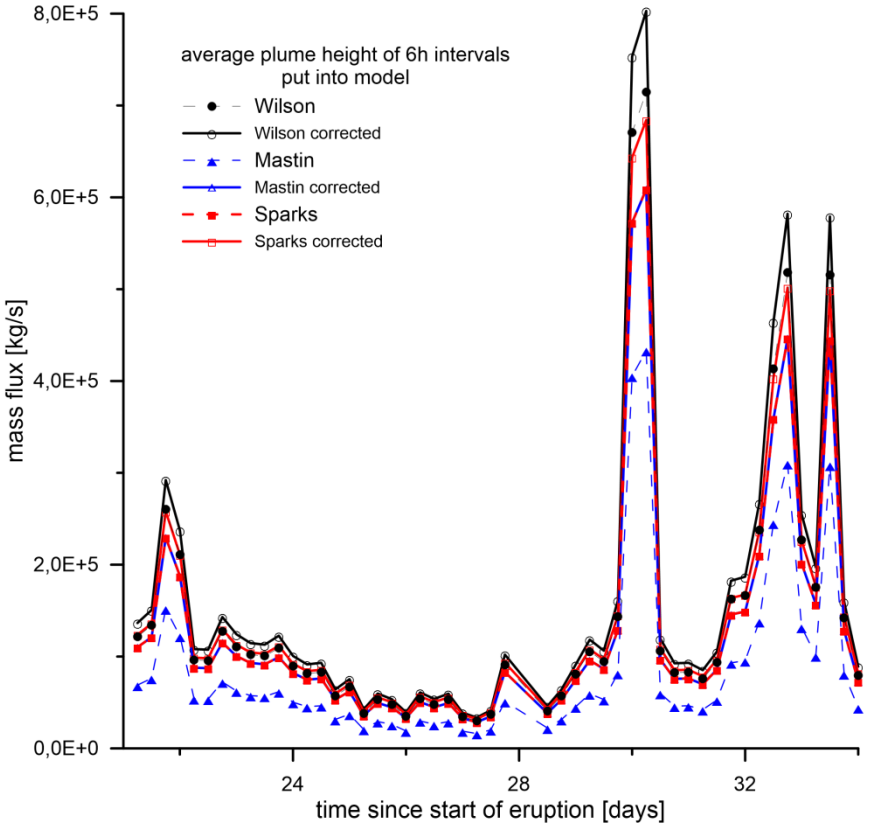

Figure 22: Mass flux for the three models used to evaluate the feasibility of using 6h averages.

Comparison of mapped fallout with model predictions

With the corrected data set, the mass erupted during all four phases was calculated by the six simple mass flux models. Figure 23 illustrates the temporal evolution of accumulated mass during each of the four main eruptive phases. Additionally, at the end of each stage the range of the mapped fallout mass (according to Gudmundsson et al 2012) is displayed.

Further details are provided by Table 2 where the first phase has been split into two parts (Ia and Ib). This is possible because the wind conditions allowed the division into the two parts, with Ia being 14-16 April when the plume was directed east, and Ib 17-18 April when the plume was directed south (Gudmundsson et al. 2012). Furthermore the output of the numerical model from Woodhouse et al. (2013) is presented, which considers the wind conditions given at the respective days. This model seems to overestimate the erupted mass by a factor in the range 6 - 13.

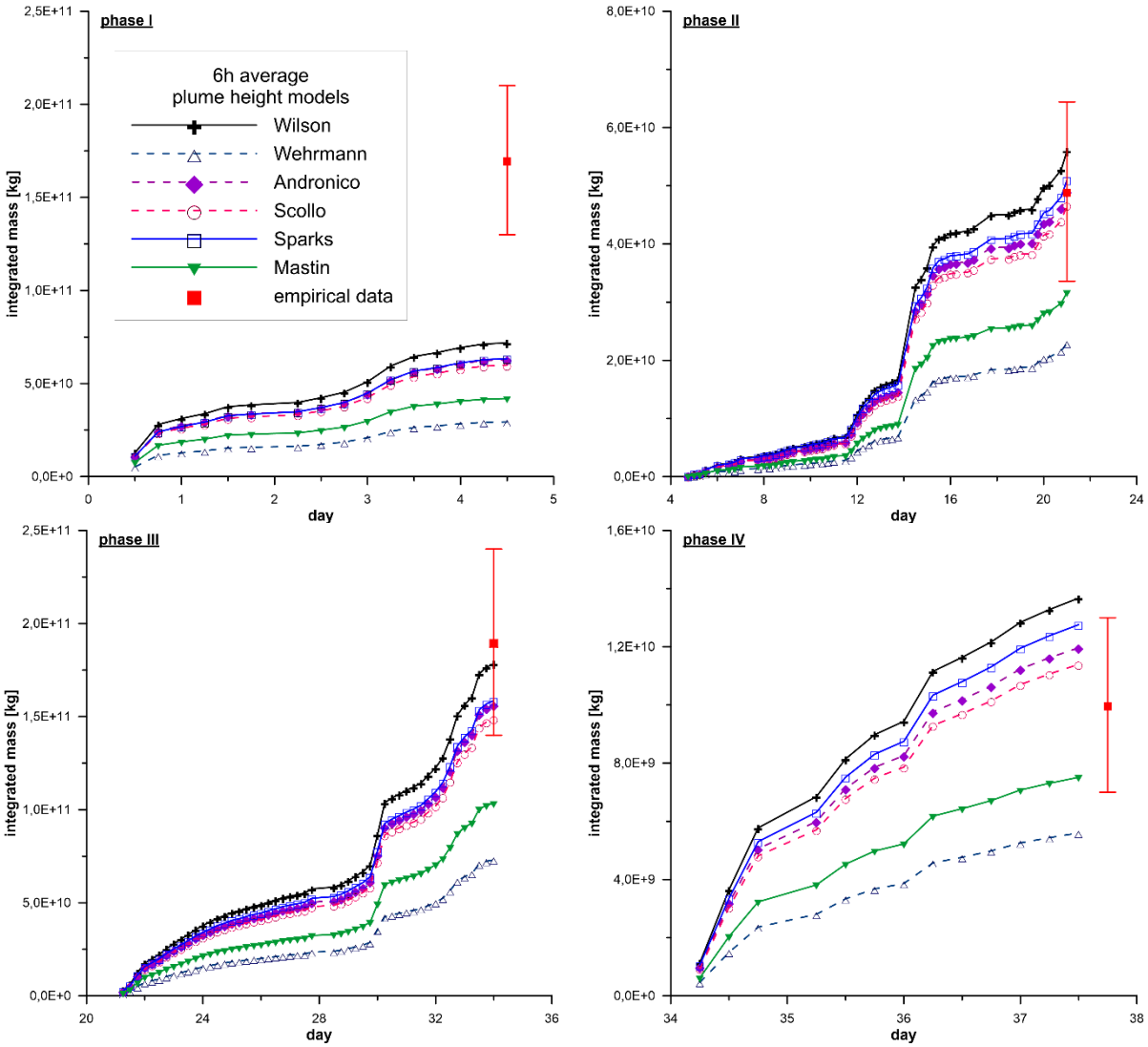

Figure 23: The predicted accumulated mass erupted using the six simple plume models for the four phases of the Eyjafjallajökull eruption (I: 14-18.04., II: 18.04-04.05, III: 05.05-17.05, and IV: 18.05-22.05).

Table 2: Comparison of predicted integrated mass erupted in Phases I to IV using the six simple plume models and the numerical wind-effect model of Woodhouse et al. (2013). Mapped fallout refers to the total mass deposited on land and the estimated mass of tephra fallout at sea.

	Ia **10^{11}kg**	**Ib** 10^{11}kg	**I** **10^{11}kg**	**II** 10^{11}kg	**III** **10^{11}kg**	**IV** 10^{11}kg
mapped fallout	**1.3 ± 0.3**	**0.4 ± 0.1**	**1.7 ± 0.4**	**0.5 ± 0.2**	**1.9 ± 0.5**	**0.1 ± 0.03**
Wilson	0.5	0.2	0.7	0.6	1.8	0.1
Wehrmann	0.2	0.1	0.3	0.2	0.7	0.1
Andronico	0.4	0.2	0.6	0.5	1.6	0.1
Scollo	0.4	0.2	0.6	0.5	1.5	0.1
Mastin	0.3	0.1	0.4	0.3	1.0	0.1
Sparks	0.4	0.2	0.6	0.5	1.6	0.1
Woodhouse	10.5	2.3	12.8	3.7	11.5	1.3

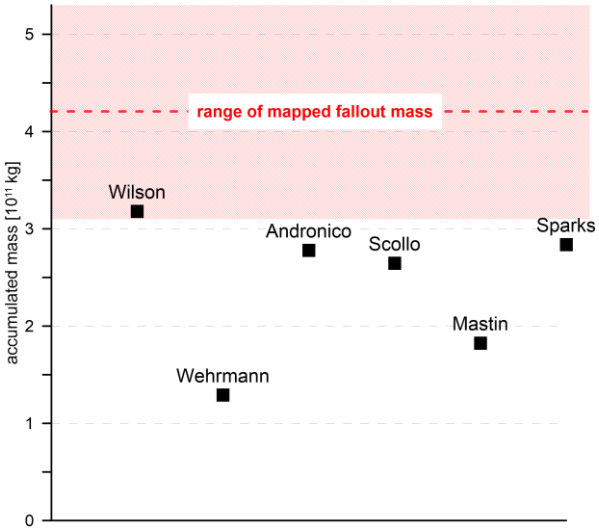

Figure 24: Comparison of mass erupted as estimated by the simple models with the total mass erupted according to Gudmundsson et al. (2012) (shaded area denotes uncertainty in total fallout). All the models give a slight underestimate. With the exception of Mastin and Wehrmann the models are very close to the lower error margins.

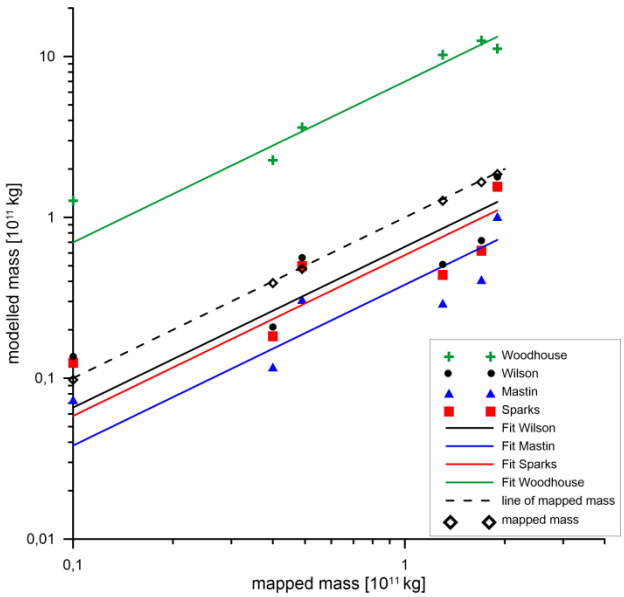

Figure 25: Comparison of mapped mass for individual phases (horizontal axis) with the Mastin, Sparks, Wilson and Woodhouse models (vertical axis).

All of the simple models underestimated the first phase which explains that also the mass erupted during the total eruption is underestimated (see Figure 24). In this context the Wilson model (which tends to provide higher values than the other simple models tested) turned out to provide values closest to the mapped fallout. However, when analyzing the four main phases separately, the Sparks model appears to give the best consistency in fitting with data.

In order to investigate if the deviation of the masses computed by plume models follow a systematic pattern, the mass values for the individual phases were plotted over the mass values of the mapped fallout (see Figure 25).

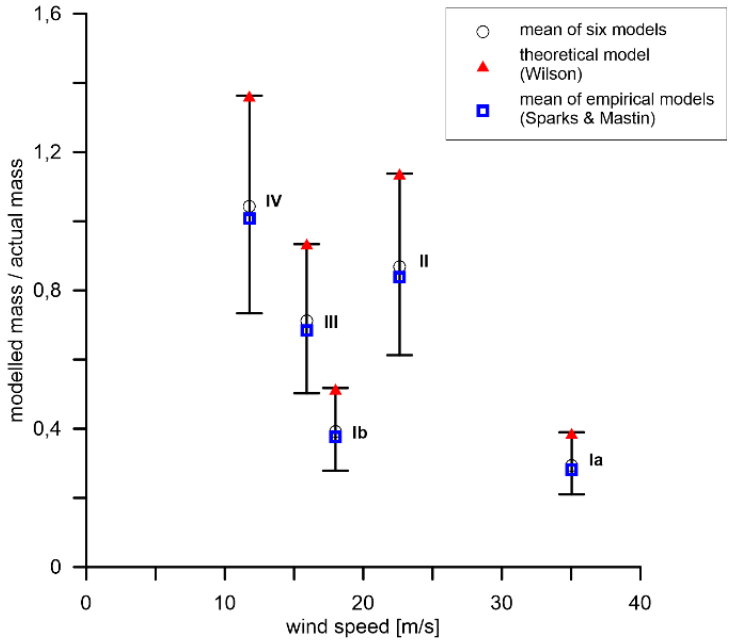

Figure 26: Ratio between modelled and mapped mass over the average wind speeds occurring at five different phases. Three combinations of the data are compared with the actual mass (fallout + estimate for the ocean part): (i) The mean values of all of the six simple models (i.e. Wilson, Wehrmann, Scollo, Andronico, Sparks and Mastin); (ii) the results of the Wilson theoretical model, and (iii) the mean values of Mastin and Sparks, representing two empirical models.

Discussion

The comparison of models presented above indicates that the simple empirical models (Sparks, Mastin) and the simple buoyant plume model (Wilson) perform reasonably well, leading to some underestimate in erupted mass. In the case of the Sparks and Wilson models the difference is not significant. For the Mastin model the difference is larger, giving about 50% of the actual fallout. In contrast the more sophisticated Woodhouse model, which attempts to incorporate the effect of wind deflection and dispersal of plume, provides a value several times the fallout-estimate of erupted material. It is unlikely that the mapped values can be off by almost a magnitude; supporting evidence such as heavy fallout at sea or at very large distances from Iceland is lacking, while considerable data suggests that the amount carried to Europe was minor (e.g. Stevenson et al., 2012, Gudmundsson et al., 2012).

It might be argued that purely empirical models, such as Sparks and Mastin do have a wind-deflection effect built into them, since in most cases some wind is present during eruptions, as e.g. demonstrated by the characteristic asymmetry in tephra deposits – that in most cases form an elongated fan in the downwind direction.

The wind effect should be visible in our data set since the mean wind was not the same for the individual phases of Eyjafjallajökull. In Figure 26 the ratio of the model-predicted mass erupted in each phase is compared to the estimated fallout from the deposits on land and their continuation out to sea. This ratio is here plotted as a function of average wind speed for the duration of the phase at 5km height (500hPa). The data do indicate a correlation, with the model-predicted mass ratio decreasing with increasing wind. A larger data set is required to resolve this issue properly and come up with a reasonably robust empirical plume discharge model incorporating wind effect.

In conclusion it can be stated that the results presented clearly indicate that the strong wind reduces plume height to some extent, leading to underestimate of mass eruption

rate for simple models based on plume height alone. The results, however, also indicate that at least some plume-discharge models that presently incorporate wind effects greatly overestimate the rate of eruption. Such models seem to require better calibration before they can be used in operational setting to estimate mass eruption rate.

Finally, the analysis presented above appears to hold considerable potential in improving the output from simple plume models. Moreover, observations of wind-deflection demonstrate that corrections are in general needed for reliable use of web-cam and other fixed location photographs to determine plume height.

References

Arason, P., Petersen G.N., Bjornsson, H. (2011): Observations of the altitude of the volcanic plume during the eruption of Eyjafjallajökull, April–May 2010. Earth Syst. Sci. Data, 3, 9-17.

Andronico, D., S. Scollo, Caruso, S., Cristaldi A. (2008): The 2002–03 Etna explosive activity: Tephra dispersal and features of the deposits, J. Geophys. Res., 113, B04209, doi:10.1029/2007JB005126.

Björnsson, H., Magnússon, S., Arason, P., and Petersen, G.N. (2013). Velocities in the plume of the 2010 Eyjafjallajökull eruption. J. Geophys. Res., 118, 11698–11711. DOI: 10.1002/jgrd.50876.

Bursik, M., Jones, M., Carn, S.,Dean, K., Patra, A., Pavlonis, M., Pitman, E.B., Singh, T., Signla, P., Webley, P., Bjornsson, H., Ripepe, M. (2012). Estimation and propagation of volcanic source parameter uncertainty in an ash transport and dispersal model: application to the Eyjafjallajokull plume of 14 – 16 April 2010. Bull. Volc., 74, 2321-2338.

Degruyter, W., Bonadonna C. (2012): Improving on mass flow rate estimates of volcanic eruptions Geophys. Res. Lett. 39 (16), doi: 10.1029/2012GL052566

Dellino, P., M. T. Gudmundsson, G. Larsen, D. Mele, J. A. Stevenson, T. Thordarson, and B. Zimanowski. (2012). Ash from the Eyjafjallajökull eruption (Iceland): Fragmentation processes and aerodynamic behavior, *J. Geophys. Res.*, 117, B00C04, doi:10.1029/2011JB008726.

Fierstein, J., Nathenson, M., 1992. Another look at the calculation of fallout tephra volumes. Bulletin of Volcanology 54, 156–167.

Gudmundsson, M.T., Thordarson, T., Höskuldsson, Á., Larsen G., Björnsson, H., Prata, A.J., Oddsson, B., Magnússon, E., Högnadóttir, T., Pedersen, G.N., Hayward, C.L., Stevenson, J.A., Jónsdóttir, I. (2012). Ash generation and distribution from the April-May 2010 eruption of Eyjafjallajökull, Iceland. Scientific Reports. 2, 572; DOI:10.1038/srep00572

Magnússon, R.L. (2012). Pixelcalc: Forrit til mælinga á stærð gosmakka út frá stafrænum myndum (in Icelandic: Pixelcalc: Software to measure height of eruption plumes from digital photos). RH-08-2012. 15 pp.

Mastin, L.G., Guffanti, M., Servranckx, R., Webley, P., Barsotti, S., Dean, K., Durant, A., Ewert, J.W., Neri, A., Rose, W.I., Schneider, D., Siebert, L., Stunder, B., Swanson, G., Tupper, A., Volentik, M., Waythomas, C.F. (2009): A multidisciplinary effort to assign realistic source parameters to models of volcanic ash-cloud transport and dispersion during eruptions, J. Volcanol. Geotherm. Res., 186, 10 – 21, doi:10.1016/j.jvolgeores.2009.01.008.

Morton, B.R., Taylor, G.I., Turner, J.S. (1956). Turbulent gravitational convection from maintained and instantaneous sources. Proc Roy Soc Lond, Ser A, Math Phys Sci A234, 1 – 23.

Oddsson, B., Gudmundsson, M.T., Larsen, G., Karlsdóttir, S. **2012.** Monitoring the plume from the basaltic phreatomagmatic 2004 Grímsvötn eruption – application of weather radar and comparison with plume models. Bull. Volc. 74, 1395-1407. DOI:10.1007/s00445-012-0598-9.

Pyle, D.M. (1989). The thickness, volume and grainsize of tephra fall deposits. Bulletin of Volcanology 51, 1–15.
Scollo, P., Del Carlo, P., Coltelli M. (2007): Tephra fallout of 2001 Etna flank eruption: Analysis of the deposit and plume dispersion, J. Volcanol. Geotherm. Res., 160, 147– 164.
Sparks, R.S.J. , Bursik, M.I., Carey, S.N., Gilbert, J.S., Glaze, L.S., Sigurdsson, H., Woods A.W. (1997): Volcanic Plumes, John Wiley & Sons, Chichester; 574 pp.
Stevenson, J.A., Loughlin, S., Rae, C., Thordarson, T., Milodowski,A.E., Gilbert,J.S., Harangi, S., Lukács, R., Højgaard, B., Árting, B., Pyne-O ' Donnell, S., MacLeod, A., Whitney, B., Cassidy, M. Distal deposition of tephra from the Eyjafjallajokull 2010 summit eruption. J. Geophys. Res, 117. JB008904.
Thorarinsson, S., 1954. The tephra fall from Hekla on March 29th, 1947. The eruption of Hekla 1947-1948 2, 1–78.
Thorkelsson, B. (ed.). The 2010 Eyjafjallajökull eruption, Iceland. Report to ICAO. University of Iceland, the National Commissioner of the Icelandic Police, The Icelandic Metorological Office. 206 pp.
Wehrmann, H., Bonadonna, C., Freundt, A., Houghton, B.F., Kutterolf S. (2006): Fontana Tephra: A basaltic plinian eruption in Nicaragua, in Volcanic Hazards in Central America, edited by W. I. Rose et al., Spec. Pap. Geol. Soc. Am., 412, 209–223.
Wilson, L., Walker, G.P.L. (1987) Explosive volcanic eruptions—VI. Ejecta dispersal in plinian eruptions: the control of eruption conditions and atmospheric properties. Geophys J R astr Soc; 89: pp. 657-679.
Woodhouse, M.J., Hogg, A.J., Phillips, J.C., and Sparks, R.S.J. (2013): Interaction between volcanic plumes and wind during the 2010 Eyjafjallajökull eruption, Iceland, J. Geophys. Res., 118, 1 – 18, doi:10.1029/2012JB009592.